SKB

Implementation of the equivalent flow rate model in DarcyTools for estimating solute transport from a damaged canister

Pirouz Shahkarami

Michel Ferry

SVENSK KÄRNBRÄNSLEHANTERING

Implementation of the equivalent flow rate model in DarcyTools for estimating solute transport from a damaged canister

Pirouz Shahkarami, Kemakta Konsult AB

Michel Ferry, MFRDC

Update notice

The original report, dated September 2024, was found to contain factual errors which have been corrected in this updated version. The corrected factual errors are presented below.

Updated 2025-05

Location	Original text	Corrected text
Page 54, App C, Eq C-18	$(\sqrt{u})_{eq} = \frac{1}{H} \times \sum_{i=1}^{nf} b_f \sqrt{u} = \frac{1}{H} \times \sum_{i=1}^{nf} \sqrt{b_f \frac{Q_f}{\sqrt{a_f}}} \approx \theta_M \times U_M$	$(\sqrt{u})_{eq} = \frac{1}{H} \times \sum_{i=1}^{nf} b_f \sqrt{u} = \frac{1}{H} \times \sum_{i=1}^{nf} \sqrt{b_f \frac{Q_f}{\sqrt{a_f}}} \approx \sqrt{\theta_M \times U_M}$
Page 54, App C, Eq C-19	$\sum_{i=1}^{nf} \sqrt{b_f \frac{Q_f}{\sqrt{a_f}}} \approx \theta_M \times U_M \times H^2$	$\sum_{i=1}^{nf} \sqrt{b_f \frac{Q_f}{\sqrt{a_f}}} \approx \sqrt{\theta_M \times U_M \times H^2}$

Summary

This report presents a comprehensive study on the equivalent flow rate model (Q_{eq}) and its efficacy in both 2D and 3D domains for solute transport calculation from a damaged canister. The primary focus of the report is the implementation and formulation of the Q_{eq} model withing an Equivalent Continuum Porous Medium (ECPM) model framework using DarcyTools. The first part of the report provides an in-depth analysis of the fundamental concepts underlying the Q_{eq} model and details its integration into the DarcyTools platform. Subsequently, the efficacy of the Q_{eq} model is investigated in a 2D domain, by performing sensitivity analyses on parameters such as the Péclet number and wall grid size. The key findings and their implications derived from these analyses are highlighted and discussed. Building on these findings, next, the Q_{eq} model's performance is evaluated in a 3D domain, focusing on various intersection scenarios. The results obtained demonstrate the model's adaptability and accuracy across diverse geometrical configurations. Finally, to conclude this study, the report showcases the application of DarcyTools and the Q_{eq} model in a large-scale repository model featuring 50 deposition holes. Both Q_{eq1} and Q_{eq2} estimations are provided, demonstrating good agreement with ConnectFlow results. This study underscores the potential of DarcyTools and the Q_{eq} model for safety assessment applications in geological repositories.

Sammanfattning

Denna rapport presenterar en omfattande studie om den ekvivalenta flödesmodellen (Q_{eq}) och dess effektivitet i både 2D- och 3D-domäner för beräkningar av ämnestransport från en skadad kapsel. Huvudfokus i rapporten är implementeringen och formuleringen av Q_{eq}-modellen i en Ekvivalent Poröst Kontinuum Medium (ECPM) modell med hjälp av DarcyTools, ett kraftfullt verktyg för att simulera flöde i porösa medier. Den första delen av rapporten ger en djupgående analys av de grundläggande begreppen i Q_{eq}-modellen, följt av dess implementering och formulering med hjälp av DarcyTools. Därefter undersöks effektiviteten av Q_{eq}-modellen i en 2D-domän, inklusive en känslighetsanalys av Péclet-talet och väggarnas rutstorlek. De viktigaste slutsatserna från dessa analyser lyfts fram och diskuteras. Nästa steg är att utvärdera Q_{eq}-modellens prestanda i en 3D-domän, med fokus på olika skärningsscenarier. De huvudsakliga resultaten från dessa scenarier presenteras, vilket visar modellens anpassningsförmåga och noggrannhet i olika geometriska konfigurationer. Slutligen visar rapporten användningen av DarcyTools och Q_{eq}-modellen i en storskalig depåmodell bestående av 50 deponeringshål. Både Q_{eq1}- och Q_{eq2}-uppskattningar tillhandahålls och visar en god överensstämmelse med ConnectFlow-resultaten. Denna studie betonar potentialen för DarcyTools och Q_{eq}-modellen för prestandabedömning av geologiska förvar.

Contents

1 Introduction and overview

The Swedish Nuclear Fuel and Waste Management Company (SKB) is currently investigating the application of DarcyTools to calculate performance measures (PMs) of radioactive waste repositories in future safety assessments. The PM to be considered in this study is the equivalent flow rate, Q_{eq}, which represents the transport ability of a fracture, or a fracture set that intersect a deposition hole, for a given concentration difference.

1.1 Safety assessment of geological repositories

The safety assessment (SA) of a geological repository is to use mathematical models to predict the long-term behaviour of radionuclide transport through the natural and engineered barriers in the given repository. The SA analysis is widely regarded as an essential tool to ensure the permanent and safe disposal of radioactive waste. The SA results can help to analyse and evaluate the extent to which the final repository complies with the established requirements and standards and thus help to build confidence in the proposed repository design. The SA analysis can help to determine the consequences in scenarios when one or more of the barriers protecting the nuclear waste fail and radioactive substances start releasing to the surrounding bedrock.

For the SA purposes, the repository system is conceptually divided into a near-field (NF) and a far-field (FF). The repository near-field, depicted schematically in Figure 1-1, comprises the fuel matrix, copper canister, and bentonite clay. Additionally, Figure 1-1 shows part of the surrounding geosphere that is damaged by excavating operations, a.k.a., excavation damaged zone (EDZ). The repository far-field, on the other hand, is the naturally fractured part of the geosphere, i.e., the host bedrock that is not significantly affected by human activities.

Should the canister fail, radionuclides would be released from the canister and begin migrating toward the biosphere. In the repository nearfield, release of radionuclides is controlled by dissolution of the fuel matrix, transport through the canister damage, diffusion through the bentonite clay, as well as adsorption and radioactive decay. After escaping from the near-field, the nuclides may further migrate in the repository far-field, where different mechanisms control their transport behaviour.
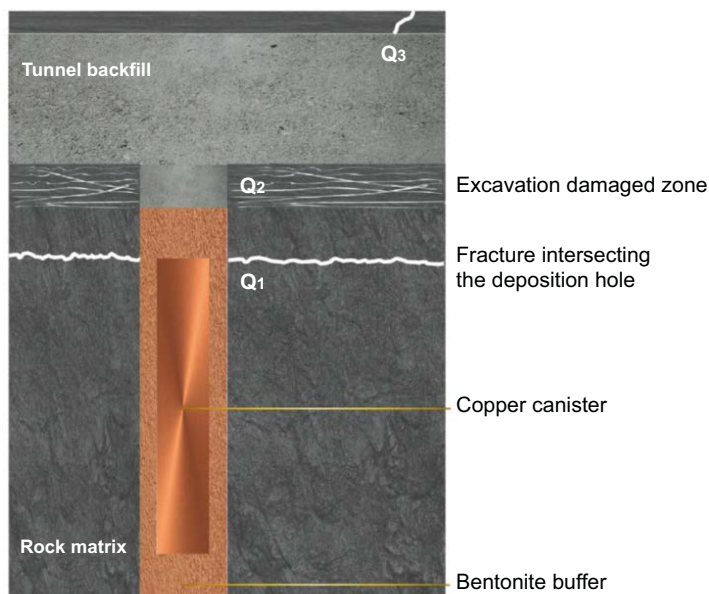

Figure 1-1. Schematic picture of the repository near-field and possible pathways that radionuclides can migrate into flowing water in fractures: into the fracture intersecting the deposition hole (Q1), into the excavation damaged zone (Q2), and into the fracture intersecting the deposition tunnel (Q3).

To assist in estimating the amount of solute that can be transported from a damaged canister by flowing water in fractures in the rock, the concept of equivalent flow rate, Q_{eq} [m³/s], was introduced (Romero, 1995). This parameter represents a fictitious flow of water which carries with it a concentration equal to that on the outer surface of the bentonite buffer. The goal is to evaluate the rate of solute transport from the canister to the flowing water in fractures and the excavation damaged zone, which are key inputs to far-field transport models. Figure 1-1 shows three possible pathways that radionuclides can migrate into flowing water in fractures from a canister, and their associated equivalent flow rates, namely, Q_1: equivalent flow rate due to the fracture intersecting the deposition hole; Q_2: equivalent flow rate due to the excavation damaged zone; Q_3: equivalent flow rate due to the fracture intersecting the deposition tunnel.

The equivalent flow rate for the transfer from the outer surface of the buffer to the water flowing in the fractured rock can be determined by assessing how far out in the flowing water the solute can diffuse during the time the water is in contact with the buffer. This is further discussed in the following section.

1.2 The basic concepts of the equivalent flow rate model

When a canister is surrounded by highly compacted bentonite clay, advection may be neglected compared to diffusive mass transport through the bentonite buffer. Therefore, in the vicinity of the buffer, if the deposition hole is intersected by a high-permeable fracture in the surrounding rock or if the surrounding rock is damaged, the water flowing in the fracture and the damaged zone will take up solutes from the buffer by diffusion, as illustrated in Figure 1-2.

During the time the flowing water with the concentration c_w [mol/m³] is in contact with the bentonite buffer, the water is exposed to the concentration at the water-buffer interface, C_0 [mol/m³]. Therefore, the longer the water contact time with the buffer, the more solute can be transferred to the flowing water. We intend to assess how much solute can be transported out of the system by introducing the concept of equivalent flow rate, Q_{eq} [m³/s], such that the transport rate, N [mol/s], can be expressed as:

$$N = Q_{eq}(C_0 - c_w) \qquad\qquad (1-1)$$

Such an approach has been presented earlier for solute transport between seeping water in fractured rock and a copper canister embedded in a clay buffer (Neretnieks et al. 2010). In what follows, a simplified model is presented to describe the above system and quantify the equivalent flow rate. In the model, the curvature of the buffer circular surface is flattened, and the flow is linear. A further simplification is made by neglecting the diffusion in the x-direction along the fracture. We explore two cases, where the available penetration depth for solute particles into the water is a) small and b) very large compared to the distance along the fracture. Figure 1-3 depicts the simplified model used to conceptualize the system. In these cases, we assume that water flows through porous media.
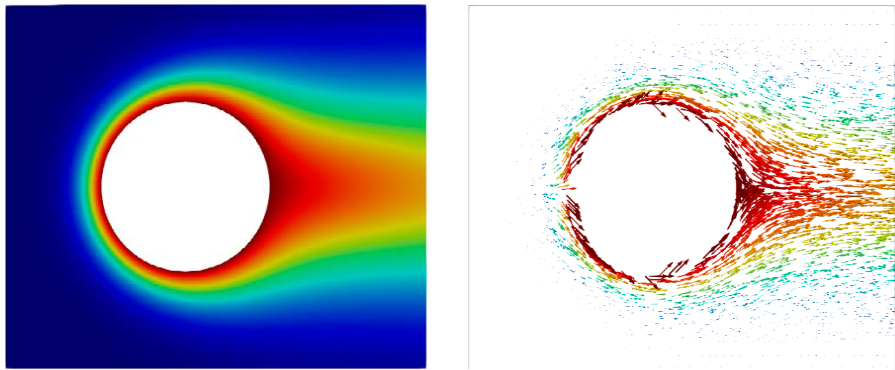

Figure 1-2. *Concentration profile and velocity vectors for the transport from a circular shape buffer to the flowing water in the fracture (top view). The colour on the plot corresponds to the concentration. Mesh resolution of the studied system can be found in Figure 2-1.*
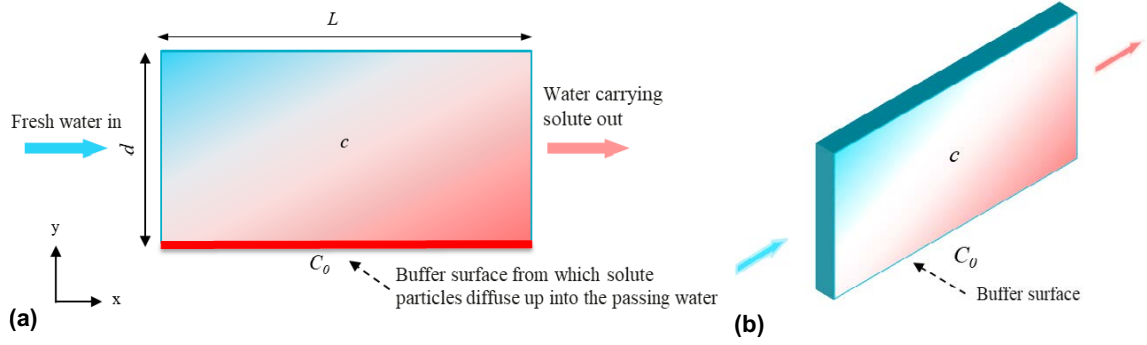
Figure 1-3. *Diffusive transport from the flattened buffer surface to the flowing water in the fracture with a limited available penetration depth, viewed from 2D (a) and 3D (b) perspectives.*

While fractures are typically considered as fully open pathways, this assumption allows us to create a general framework that can also account for variations in permeability and obstruction within fractures, as may occur in a damaged zone surrounding a deposition tunnel. It's important to note that later in the report, we assume that fractures remain fully open.

1.2.1   Limited available penetration depth (Flat surface)

We study a one-dimensional diffusive transport within a porous domain[1] with an initial concentration of $C = c_w$. At time t > 0, a concentration of C_0 is introduced at the surface, as depicted in Figure 1-3. The aim is to analyse the evolution of the concentration profile over time, which is analogous to the process of examining how rapidly the concentration between the two farthest surfaces at $y = 0$ and $y = d$ will equalize with time. In the case of a stationary system, where the concentration varies only spatially and not temporally, the mass balance equation for a non-sorbing nuclide in the domain can be expressed as:

$$u \frac{\partial c}{\partial x} = D_p \frac{\partial^2 c}{\partial y^2} \tag{1-2}$$

u represents the true fluid velocity, D_p [m²/s] denotes the pore diffusivity, and x is the spatial coordinate along the direction of flow in the domain. Equation (1-2) can be reformulated as:

$$\frac{\partial c}{\partial (x/u)} = D_p \frac{\partial^2 c}{\partial y^2} \tag{1-3}$$

Or alternatively,

$$\frac{\partial c}{\partial t_{res}} = D_p \frac{\partial^2 c}{\partial y^2} \tag{1-4}$$

where t_{res} [s] denotes water residence time in contact with the surface defined as:

$$t_{res} = \frac{x}{u} = \frac{x\varepsilon}{U_d} \tag{1-5}$$

Here, U_d denotes the Darcy flux[2], and ε represents porosity defined as the ratio of the pore volume to total volume of the porous domain, i.e. fracture.

---

[1] Noting that the porous domain represents a fracture or a damaged zone.

[2] Volume rate of flow through a unit cross-sectional area of the solid (fracture infilling) plus water (pores).

The boundary conditions for (1-5) are:

$$c = C_0 \quad \text{at } y = 0$$

$$\frac{\partial c}{\partial y} = 0 \quad \text{at } y = d$$

By incorporating the initial and boundary conditions, it is possible to derive an exact analytical solution to Equation (1-4). This solution can be expressed as (Bird et al. 2002, Second Edition, p 377):

$$\frac{c - c_w}{C_0 - c_w} = 1 - 2 \sum_{n=0}^{\infty} \frac{(-1)^n}{(n+1/2)\pi} e^{-T(n+1/2)^2\pi^2} \cos\left((n+1/2)\pi\left(1 - \frac{y}{d}\right)\right) \tag{1-6}$$

T is the dimensionless group characterizing the spreading rate of solute, defined as:

$$T = \frac{t_{res}}{d^2/D_p} = \frac{t_{res}}{t_{dif}} = \frac{1}{\text{Pe}} \tag{1-7}$$

In fact, T represents the inverse of the Péclet number, Pe, and is commonly referred to as the dispersion number. The mean concentration c_m can also be obtained by integration over the distance from y = 0 to y = d to give:

$$\frac{c_m - c_w}{C_0 - c_w} = 1 - 2 \sum_{n=0}^{\infty} \frac{(-1)^n}{(n+1/2)\pi} e^{-T(n+1/2)^2\pi^2} \sin\left((n+1/2)\pi\right) \tag{1-8}$$

The results, as shown in Figure 1-4, demonstrate the evolution of the concentration distribution in the y-direction as the contact time increases. In addition, the mean concentration variation in the domain over the dimensionless group T is demonstrated in Figure 1-5. When the dimensionless group T reaches a critical value, marked as $T_{crit} = 1.12$, the mean concentration deviates from C_0 by mere 5 %. This finding suggests that for T values greater than or equal to 1.12, the mean concentration (c_m) can be considered practically identical to the surface concentration, indicating a well-mixed state, resulted from the diffusion process. Consequently, it can be inferred that in this case the equivalent flow rate is approximately equal to the actual volumetric flow rate within the fracture.

Figure 1-4. *Concentration distribution in the y-directions, with a limited available penetration depth, with $c_w = 0$.*
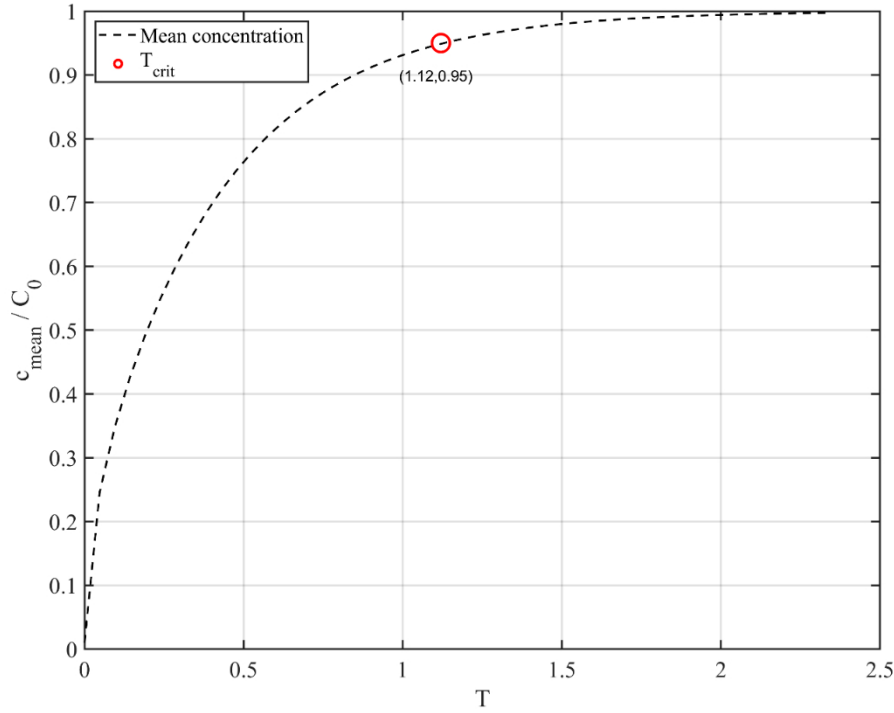
Figure 1-5. *Mean concentration evolution over time, with a limited available penetration depth, with c_w= 0.*

Hence, one can estimate the full-mixing time, which refers to the time taken for the domain to reach a state of well-mixed condition, denoted as t_{mix}.

$$t_{mix} = 1.12 \frac{d^2}{D_p} \tag{1-9}$$

Therefore, if t_{res} is equal or larger that t_{mix}, Q_{eq} can safely be assumed to be equal to the water volumetric flow rate, Q [m³/s].

1.2.2 Large available penetration depth (Flat surface)

For relatively short residence times such that the tip of the concentration profile has not yet reached the outer boundary at $y = d_{FS}$, i.e., when d_{FS} is very large as depicted in Figure 1-6 and Figure 1-7, the solute concentration profile in the water, Equation (1-6) above, can be approximated as (Bird et al. 2002, Second Edition, p 117):

$$\frac{c^{FS} - c_w}{C_0 - c_w} = erfc \sqrt{\frac{y^2}{4D_p t_{res}}} \tag{1-10}$$

where FS stands for the **F**racture in the **S**urrounding rock.
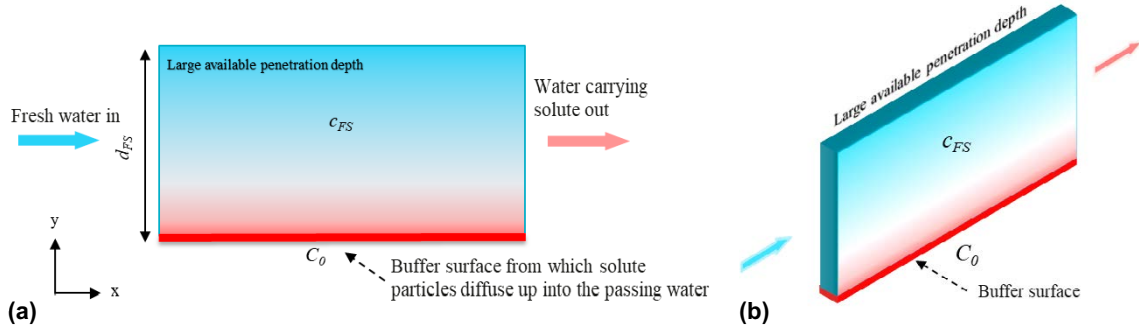
Figure 1-6. *Diffusive transport from the buffer surface to the flowing water with a large available penetration depth, viewed from 2D (a) and 3D (b) perspectives.*
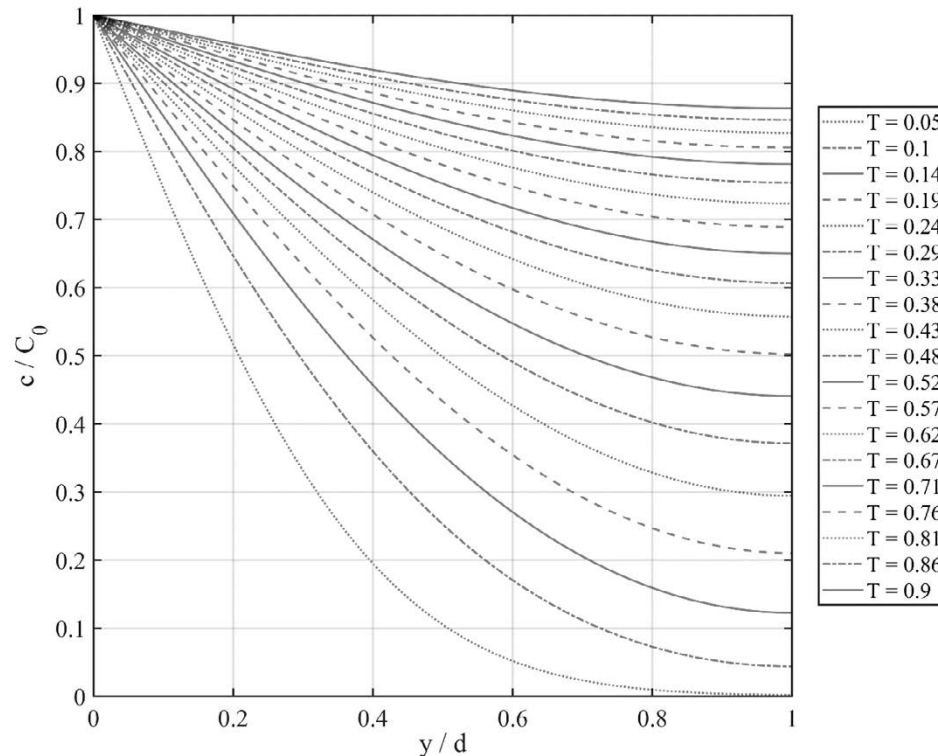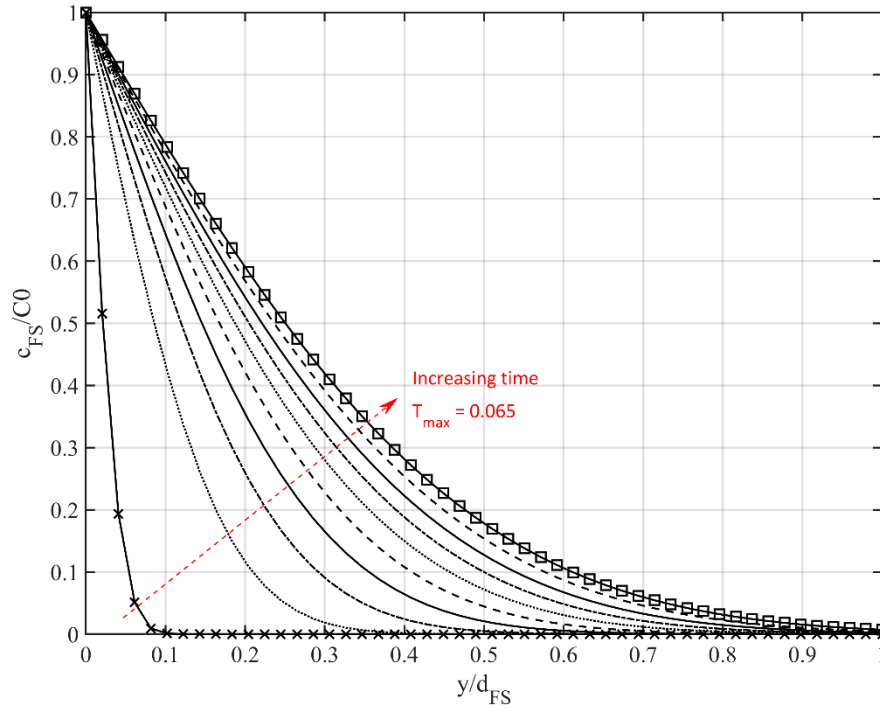

Figure 1-7. *Concentration distribution in the y-direction, with a large available penetration depth, with $c_w = 0$.*

The mean concentration, c_{mean}^{FS}, can then be obtained by integrating the concentration profile from the buffer surface ($y = 0$) to infinity ($y = d_{FS}$), to give:

$$\frac{c_{mean}^{FS} - c_w}{C_0 - c_w} = \frac{\eta_{mean}^{FS}}{d_{FS}} = \frac{\sqrt{\frac{4D_p t_{res}}{\pi}}}{d_{FS}} \tag{1-11}$$

Hence, the mean penetration depth of the solute into the flowing water can be determined using the following equation:

$$\eta_{mean}^{FS} = \sqrt{\frac{4D_p t_{res}}{\pi}} \tag{1-12}$$

The parameter η_{mean}^{FS} characterizes the mean distance from the interface between flowing water and buffer at which solute exchange can occur within the given contact time. The visual representation of this mean penetration depth is denoted by the width of the red region in Figure 1-6.

1.3　Analytical solution for mass transfer from a flat surface

In Figure 1-6, the water flow rate within the mean penetration depth is considered the equivalent flow rate, Q_{eq}, which accounts for the solute uptake from the surface. Mathematically, Q_{eq} can be expressed using Equation (1-13) and Equation (1-14), where Equation (1-13) links Q_{eq} to the product of the mean penetration depth η_{mean}^{FS}, the fracture thickness[3] Δ [m], and the fluid Darcy flux, U_d [m/s]. Alternatively, Equation (1-14) establishes a link between the Q_{eq} and the volumetric flow rate Q as determined by Darcy's law.

$$Q_{eq} = U_d \times \Delta \times \eta_{mean}^{FS} \tag{1-13}$$

$$\frac{Q_{eq}}{Q} = \frac{c_{mean}^{FS} - c_w}{C_0 - c_w} = \frac{\eta_{mean}^{FS}}{d_{FS}} \tag{1-14}$$

In other words, the well-mixed condition $(C_0 - c_w)$ in the fracture over distance η_{mean}^{FS} yields the same mass in the fracture as the entire concentration profile in the y-direction. By substituting the variable t_{res} with its respective definitions from Equation (1-5), Equation (1-13) can be reformulated to provide the following expression:

$$Q_{eq} = U_d \times \Delta \times \sqrt{\frac{4D_p t_{res}}{\pi}} = \frac{2}{\sqrt{\pi}} \times \Delta \times \sqrt{U_d D_e L} \tag{1-15}$$

where L [m] represent the distance travelled by the fluid in the direction of flow. When a fracture intersects a deposition hole, the travel distance can be estimated as the length of the intersection between the deposition hole and the fracture[4]. D_e is the effective diffusivity, expressed as

$$D_e = D_p \times \varepsilon \tag{1-16}$$

By substituting Equation (1-14) into Equation (1-1), the solute transport rate, N, can be expressed as:

$$N = Q_{eq}(C_0 - c_w) = Q(c_{mean}^{FS} - c_w) \tag{1-17}$$

It should be emphasized that Equations (1-10) and (1-12) hold true under specific conditions, primarily when the residence time remains relatively short, preventing the concentration profile's tip from reaching the outer boundary. In practice, as illustrated in Figure 1-7 with a solid line and square markers (□), this condition is met when (T ≤ 0.065) or equivalently when Pe ≥ 15.4). Alternatively, by employing Equation (1-12), this condition holds when the η_{mean}^{FS} is approximately 3.5 times smaller than the d_{FS}. This conclusion is derived by comparing the complete solution provided by Equation (1-6) with the approximate solution of Equation (1-10).

Furthermore, in cases where the Péclet number becomes excessively large, the concentration profile fails to develop due to extremely brief contact time between flowing water and the flat surface. To provide a rough estimate of the maximum allowable Péclet number, ensuring the presence of a concentration profile, one may assume that this condition is met when the concentration profile extends up to 10 % of the diffusion depth, d_{FS}, as shown in Figure 1-7 with a solid line and cross markers (×). Under this assumption, the minimum T required is $T = 5e^{-4}$, corresponding to a maximum Péclet number Pe < 2 000. Alternatively, if one assumes an extension of 50 % rather than 10 % for the concentration profile, the maximum allowable Péclet number becomes 64, Pe < 64. It is important to bear in mind, as discussed earlier in Section 1.2.1, that when the dimensionless group T equals or exceeds $T_{crit} = 1.12$, diffusion effectively evens out the concentration in the direction of diffusion. Consequently, the equivalent flow rate can be approximated by the actual flow rate.

---

[3] Δ represents the distance between the two fracture (or damaged zone) surfaces.

[4] Note that if the deposition hole is entirely contained within the fracture, a factor of 2 should be included to consider that fluid passes on both sides of the deposition hole.

1.4 Analytical solution for mass transfer from a circular cylinder

As discussed above, the estimation of solute transport rate by diffusion and advection from a flat surface can be achieved using Equation (1-15). Nevertheless, this expression has limitations when applied to curved surfaces such as a cylinder-shaped deposition hole, primarily because it straightens out the curvature of the surface. Specifically, it neglects diffusion in the flow direction and velocity differences among adjacent streamlines close to the deposition hole. To address these limitations, an alternative solution for solute transport from a deposition hole with a curved surface has been developed by Chambré et al. (1982). This solution, Equation (1-18), overcomes the shortcomings of Equation (1-15) and provides a more accurate depiction of solute transport. It is worth noting that this solution is applicable when the Péclet number exceeds 4:

$$Q_{eq} = 2 \times \frac{4}{\sqrt{\pi}} \times \Delta \times D_e \sqrt{Pe} \qquad (1\text{-}18)$$

Given the cylinder-shaped deposition hole, the Péclet number can be defined in terms of the radius of the deposition hole, R, as follows:

$$Pe = \frac{U_d R}{D_e} \qquad (1\text{-}19)$$

Note that the *factor 2* in Equation (1-18) comes from the fact that fluid passes both sides of the deposition hole. Utilizing the definitions of Pe and D_e, as provided in Equations (1-19) and (1-16) respectively, it is possible to reformulate Equation (1-18) as follows.

$$Q_{eq} = 8\Delta \times \sqrt{\frac{R}{\pi}} \times \sqrt{U_d \varepsilon D_p} = 8\Delta \times \sqrt{\frac{R}{\pi}} \times \sqrt{U_d D_e} \qquad (1\text{-}20)$$

It is also important to note that in the formulations outlined above fracture, or a damaged zone, is represented as an equivalent porous medium characterized by a porosity ε. In cases where the fracture is considered fully open ($\varepsilon = 1$), U_d is constrained within the open fracture and therefore equals the true flow velocity, $U_d = u$. Thus, Equation (1-20) reduces to Equation (1-21).

$$Q_{eq-Analytical} = 8b \times \sqrt{\frac{U_d D_w R}{\pi}} \qquad (1\text{-}21)$$

- b represents the aperture of the fracture that is fully open[5] [m].
- R is the deposition hole radius [m].
- D_w denotes the diffusivity in water [m^2/s].
- U_d represents the flow velocity[6] in the fracture [m/s].

It should be emphasized that in all the simulation that are presented hereafter, it is assumed that the fracture is fully open with $\varepsilon = 1$. Further elaboration on the effective diffusivity, D_e, and how it is treated in DarcyTools can be found in Appendix A.

---

[5] Thus, the fracture thickness equals its aperture, $b = \Delta$.

[6] In this case, U_d equals the true flow velocity in the fracture, u.

1.5 Semi-analytical solution for ECPM representation of fractures in DarcyTools

Consider a cylindrical deposition hole that is intersected by a single discrete fracture, f, at a right angle, as depicted in Figure 1-8(a). The analytical expression, Equation (1-21), can be employed to determine the amount of solute that can be transported through the fracture, Q_{eq}^f,

$$Q_{eq}^f = \frac{8\sqrt{D_w R}}{\sqrt{\pi}} b_f \times \sqrt{U_{d,f}} \qquad (1\text{-}22)$$

where b_f and $U_{d,f}$ represents the aperture and Darcy flux in the fully open fracture, f. In the case where the deposition hole is intersected by multiple fractures at a right angle, as illustrated in Figure 1-8(b), the total equivalent flow rate can be determined by summing the individual equivalent flow rates of each intersecting fracture leading to:

$$Q_{eq-DFN} = \sum_{f=1}^{nf} Q_{eq}^f = \frac{8\sqrt{D_w R}}{\sqrt{\pi}} \times \sum_{i=1}^{nf} b_f \sqrt{U_{d,f}} \qquad (1\text{-}23)$$

or equivalently

$$Q_{eq-DFN} = \frac{8\sqrt{D_w R}}{\sqrt{\pi}} \times \varepsilon_f H \times \frac{\sum_{f=1}^{nf} b_f \sqrt{U_{d,f}}}{\varepsilon_f H} \qquad (1\text{-}24)$$

where H is the height of the deposition hole and ε_f is a flow porosity over the deposition hole defined as:

$$\varepsilon_f = \frac{\sum_{i=1}^{nf} b_f}{H} \qquad (1\text{-}25)$$

Thus, the last term on the right-hand side of the Equation (1-24) can be interpreted as the weighted mean value of $\sqrt{U_d}$, which is denoted by $\left(\sqrt{U_d}\right)_{M-DFN}$ and is defined as:

$$\left(\sqrt{U_d}\right)_{M-DFN} = \frac{1}{\varepsilon_f H} \times \sum_{i=1}^{nf} b_f \sqrt{U_{d,f}} \qquad (1\text{-}26)$$

Hence, it is possible to rewrite Equation (1-24) as follows:

$$Q_{eq-DFN} = \frac{8\sqrt{D_w R}}{\sqrt{\pi}} \times \varepsilon_f H \times \left(\sqrt{U_d}\right)_{M-DFN} \qquad (1\text{-}27)$$

The above formulation concerns the discrete fracture network representation of the parallel fractures intersecting the deposition hole, where flow velocity[7] and apertures details of individual fractures are known.
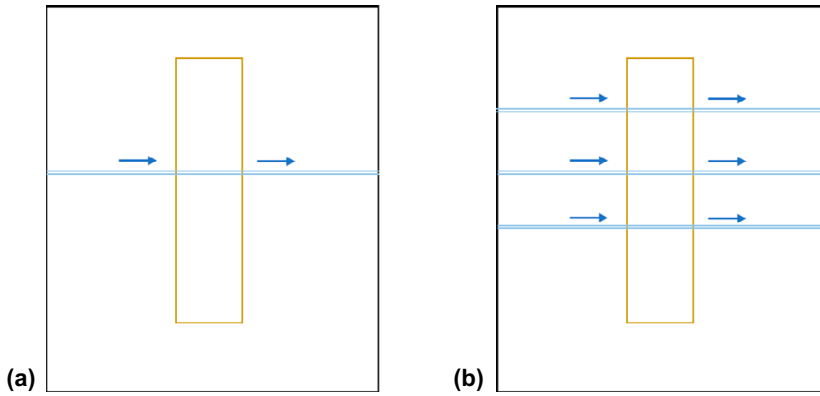

(a)   **(b)**

Figure 1-8. *Illustration of a single (a) and three (b) fracture(s) intersecting a deposition hole at a right angle.*

---

[7] ConnectFlow gives 2D Darcy flux in a fracture defined as $U_{d,f} = b_f \times u$. Flow velocity can then be calculated from the Darcy flux.

It is important to note that the DarcyTools solver relies on a finite volume method and represents fractures as an Equivalent Continuous Porous Medium (ECPM). This representation can be achieved by introducing a pre-defined fracture "object" whose properties are mapped onto the control volumes, also known as cells, within the computational domain (Ferry, 2020a). This mapping results in a series of interconnected cells representing the intersecting fracture, each assigned with different size and upscaled transport properties, including a cell porosity, θ.

In this ECPM domain, if the fracture object shown in Figure 1-8 (a) is assumed to be located in a single layer of cells with a size of η_i, then the cell porosity, denoted as θ_i, is calculated in DarcyTools using the following expression (Ferry, 2020b):

$$\theta_i = \frac{b_f}{\eta_i} \tag{1-28}$$

and DarcyTools computes the Darcy flux in the cell, U_i, as:

$$U_i = \theta_i U_{d,f} = \frac{b_f}{\eta_i} U_{d,f} \tag{1-29}$$

Subsequently, by incorporating the above cell values in Equation (1-22), we can obtain for cell i:

$$Q_{eq,i} = \frac{8\sqrt{D_w R}}{\sqrt{\pi}} \eta_i \sqrt{\theta_i U_i} \tag{1-30}$$

If we include multiple layers of cells along the cylinder to achieve a height of H, the average equivalent flow rate, $Q_{eq,\,ECPM}$ value across all cells on the deposition hole wall can be computed as:

$$Q_{eq,ECPM} = \frac{8\sqrt{D_w R}}{\sqrt{\pi}} \times H \times \sum_{i=1}^{nc} \frac{\eta_i}{H} \sqrt{\theta_i U_i} \tag{1-31}$$

or equivalently,

$$Q_{eq,ECPM} = 8H \frac{\sqrt{D_w R}}{\sqrt{\pi}} \times \left(\sqrt{\theta U}\right)_{M-ECPM} \tag{1-32}$$

here nc represents the number of cells within the ECPM representation of fracture intersections with the deposition hole and $\left(\sqrt{\theta U}\right)_{M-ECPM}$ is the mean of square root of Darcy fluxes in vicinity of the deposition hole defined as:

$$\left(\sqrt{\theta U}\right)_{M-ECPM} = \frac{1}{H} \times \sum_{i=1}^{nc} \eta_i \sqrt{\theta_i U_i} \tag{1-33}$$

It is important to acknowledge that determining $\left(\sqrt{\theta U}\right)_{M-ECPM}$ is not a straightforward process in DarcyTools. This is primarily because porosity is assigned as a cell value in DarcyTools while velocity (U) is allocated to the cell faces. To address this issue, an alternative expression, $Q_{eq\text{-}Semi\text{-}Analytical}$, has been proposed in this study to approximate $Q_{eq,ECPM}$ within the DarcyTools domain. This approach involves computing the mean Darcy flux, U_M, and mean porosity, θ_M, for all the cells associated with the ECPM representation of fracture intersections with the deposition hole. The expression is formulated as follows:

$$Q_{eq-Semi-Analytical} = 8H \sqrt{\frac{D_w R}{\pi}} \sqrt{\theta_M U_M} \tag{1-34}$$

With

$$\theta_M = \frac{\sum_{i=1}^{nc} \theta_i v_i}{\sum_{i=1}^{nc} v_i} \tag{1-35}$$

and

$$U_M = \sqrt{U_{Mx}^2 + U_{My}^2 + U_{Mz}^2} \tag{1-36}$$

where

$$U_{Mx} = \frac{1}{2}\left[\left(\frac{\iint u_x dA_x}{\iint dA_x}\right)_{east} - \left(\frac{\iint u_x dA_x}{\iint dA_x}\right)_{west}\right]$$ (1-37)

$$U_{My} = \frac{1}{2}\left[\left(\frac{\iint u_y dA_y}{\iint dA_y}\right)_{north} - \left(\frac{\iint u_y dA_y}{\iint dA_y}\right)_{south}\right]$$ (1-38)

$$U_{Mz} = \frac{1}{2}\left[\left(\frac{\iint u_z dA_z}{\iint dA_z}\right)_{high} - \left(\frac{\iint u_z dA_z}{\iint dA_z}\right)_{low}\right]$$ (1-39)

In the above equations,

- nc is the number of cells within the ECPM representation of fracture intersections with the deposition hole.

- v_i denotes the volume of cell i [m³].

- θ_i represents the porosity of cell i [-].

- u_k is the Darcy flux on the deposition hole cells' surfaces [m/s]. Subscript k denotes the flow direction.

- A_k denotes the surface area normal to the k-direction [m²].

In a simple case where a fracture f intersects the deposition hole at a right angle, θ_M becomes:

$$\theta_M = \frac{\sum \theta_i v_i}{\sum v_i} = \frac{b_f}{H}$$ (1-40)

DarcyTools then calculates U_M as:

$$U_M = \frac{b_f}{H} U_{d,f}$$ (1-41)

Hence, the Q_{eq} value of an intersecting fracture represented as an ECPM within the DarcyTools domain can be obtained by applying the expressions for U_M and θ_M to give:

$$Q_{eq-Semi-Analytical} = \frac{8\sqrt{D_w R}}{\sqrt{\pi}} b_f \times \sqrt{U_{d,f}}$$ (1-42)

This is equivalent to the analytical expression presented in, Equation (1-22). Alternatively, when two parallel and identical fractures intersect the deposition hole at a right angle, the semi-analytical solution can be expressed using the following general form:

$$Q_{eq-Semi-Analytical} = \frac{8\sqrt{D_w R}}{\sqrt{\pi}} H \times \theta_M \times \sqrt{U_{d,f}}$$ (1-43)

For this system θ_M becomes

$$\theta_M = 2\frac{b_f}{H}$$ (1-44)

Hence,

$$Q_{eq-Semi-Analytical} = 2 \times \frac{8\sqrt{D_w R}}{\sqrt{\pi}} b_f \times \sqrt{U_{d,f}} = 2 \times Q_{eq}^f$$ (1-45)

Which is correct and expected for two identical parallel fractures. Similarly, Appendix B presents a mathematical analysis that employs the Cubic law to calculate Q_{eq} for both DFN and ECPM models for single and parallel fractures with varying aperture. The analysis demonstrates that Q_{eq} values are

comparable for both single fractures and multiple parallel fractures with similar aperture and length in both DFN and ECPM models. Even for parallel fractures with varying apertures, minor deviations in aperture size result in similar Q_{eq} values for DFN and ECPM models.

Additionally, Appendix C focuses on deriving relationships between flow parameters in the DFN and ECPM formulations, particularly addressing the mean Darcy flux as it appears in the DFN formulation, $(U_d)_{M-DFN}$. The appendix explores normal and lognormal distributions for the (square root of) fracture velocity with mean μ and standard deviation σ. It is shown that within the ECPM domain near the deposition hole, $\theta_M \times U_M$ can estimate the mean Darcy flux if the variance, σ^2, is small. In Chapter 3, $\theta_M \times U_M$ is reported alongside the $Q_{eq-Semi-Analytical}$ values for different intersection scenarios.

Beyond its application in straightforward intersection scenarios, Equation (1-34) can also be employed in complex situations where multiple fractures intersect the deposition hole at various angles. However, accurately estimating the mean transport properties of the underlying fracture network that intersects the deposition hole presents a primary challenge in such cases. For further insights into this topic, refer to Chapter 3, where different intersection scenarios are investigated in a three-dimensional, 3D, domain.

2 Investigation of the Q_{eq} model's efficacy in a 2D domain

This section is dedicated to detailing the implementation of the equivalent flow rate model in a two-dimensional, 2D, domain using DarcyTools. The primary objective of this study is to determine the solute transport rate, N, using a numerical integration technique and the Q_{eq} analytical formulation, Equation (1-21). Furthermore, the study aims to identify the transport conditions that satisfy the validity of the equivalent flow rate model given the cylindrical shape of a deposition hole. The discussions presented in this section offer insights into the mathematical modelling and computational techniques employed in models presented in this study. This section specifically focuses on a relatively simpler 2D model, while later sections in this report will explore modelling efforts of more complex 3D models.

In the 2D model, the flow and transport equations are solved within the framework depicted in Figure 2-1. The model consists of a cylindrical deposition hole with a radius of 0.875 [m], which is intersected by a fracture with a thickness of 0.25 [mm]. In 2D space, the cylinder is depicted as a circular entity, and the fracture is represented by a squared permeable zone that extends 55 [m] and 50 [m] in X and Y directions, respectively. In the present study, the intersecting fracture is fully open ($\varepsilon = 1$) and is modelled with a uniform Darcy flux, U_d [m/s], in the x-direction that remains constant throughout the entire fracture. As a result, it is not necessary to create a distinct fracture "object" and map its properties on to the grid. Instead, constant permeability, pressure gradient and effective diffusivity are assigned to the entire computational domain. In this example, this results in a constant Péclet number of Pe = 50, as defined by Equation (1-19).
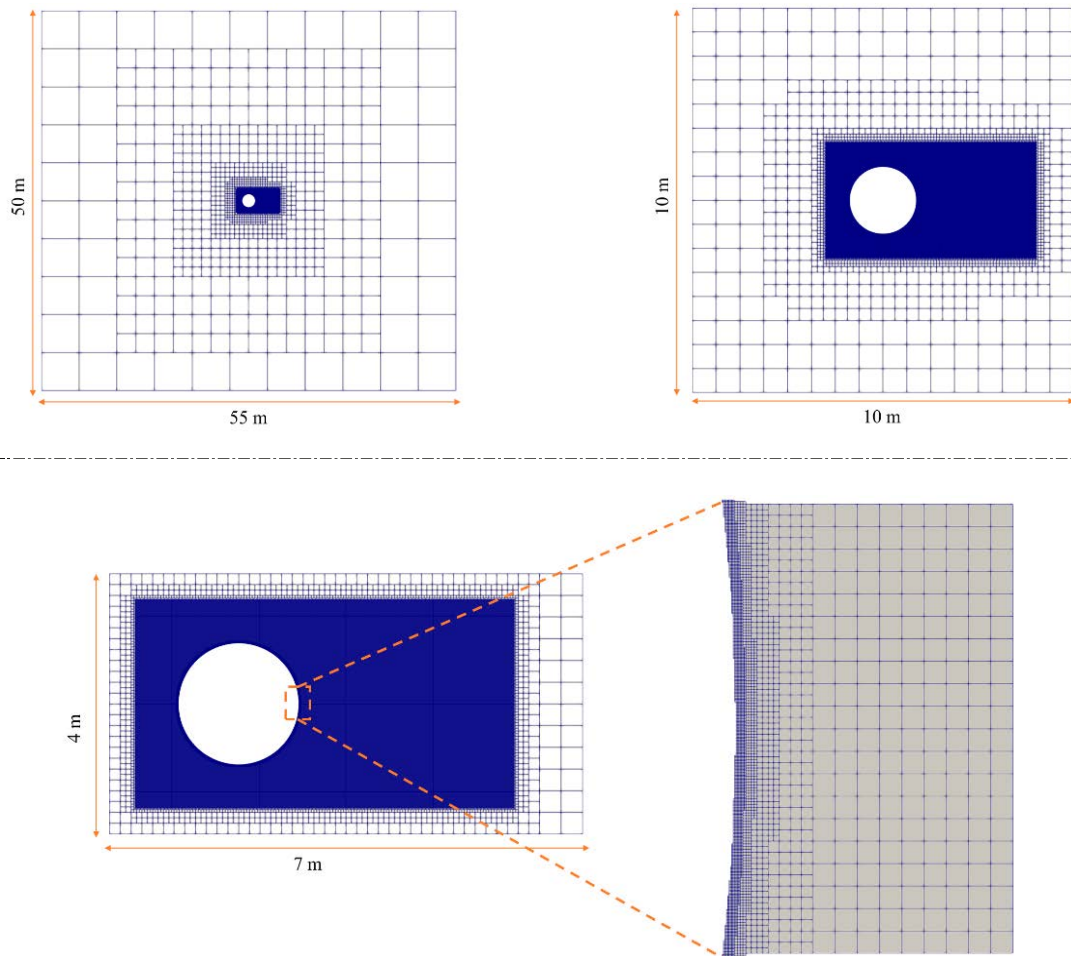
Figure 2-1. *Geometry and mesh resolution of the studied system, hollow cylinder case, in the XY plane.*

2.1 Numerical solution ($Q_{eq\text{-}Numerical}$)

In DarcyTools, the total amount of solute that is transported from a deposition hole can be calculated by numerical integration over boundary surfaces of a measurement box, as shown by the pink dashed lines in the 2D case depicted in Figure 2-2. The Q_{eq} values estimated via numerical integration are herein referred to as Q_n or $Q_{eq\text{-}Numerical}$ and is defined as:

$$Q_{eq-Numerical} = \frac{1}{C_0} \oiint C\, \vec{u}\, \vec{n}\, ds \qquad (2\text{-}1)$$

In the above equations,

- C is a solute concentration [gr/m^3].

- $\vec{u}$ is the Darcy flux vector [m/s].

- $\vec{n}$ is the normal vector[8].

The following section investigates the impact of grid size and boundary condition (BC) location on the numerical solution. Specifically, the study explores how varying the wall grid size and location of concentration boundary conditions affect the accuracy and precision of the $Q_{eq\text{-}Numerical}$. The findings from this analysis can help optimize the selection of grid size for similar problems.
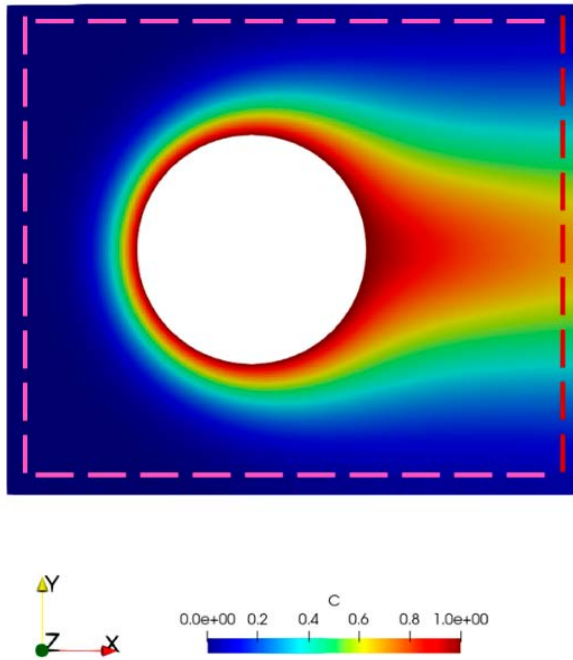
Figure 2-2. *Illustration of transport from a hollow cylinder and its measurement box (delineated by pink borders) used for capturing the transport rate, in the XY plane. The colour on the plot corresponds to the concentration.*

---

[8] The vector of the box plotted by the dashed pink line in Figure 2-2.

2.2 Effect of wall grid size and BC location on $Q_{eq\text{-}Numerical}$

From a physical standpoint, we intend to simulate a scenario where no flow occurs within the deposition hole. In DarcyTools, this system can be set up in two alternative models, where the accuracy of the numerical solution can be significantly affected by the choice of wall grid size and transport boundary conditions, particularly due to the small characteristic length of diffusion. This study, therefore, investigate the impact of wall grid size on simulation results in two cases:

1) **Hollow Cylinder Case:** In which C=1 is set on the wall cells, the interior cells of the deposition hole are eliminated, and the boundary condition C=1 is applied to the wall cells.

2) **Filled Cylinder Case:** In which the deposition hole's internal cells are preserved, but rendered non-conductive, and the boundary condition C=1 is enforced on these non-conductive internal cells.

By examining these two scenarios, our objective is to assess the extent to which variations in wall grid size affect the numerical solution, $Q_{eq\text{-}Numerical}$. The results for these scenarios at Pe = 50 are presented in Figure 2-3. Notably, altering the ratio of wall cell size to radius, Δ_{wall}/R, has no impact on the Q_{eq} values obtained from the analytical expression Equation (1-21). This is expected since the transport properties and applied radius remain constant.

In the filled cylinder case, where C=1 is applied to the inside cells, the difference between the estimated equivalent flow rate, Q_{eq}, and the calculated transport rate, Q_n, decreases as the cell size decreases. It approaches zero as the cell size approaches 0.5 % of the deposition hole radius. Larger cell sizes, however, fail to accurately capture the details of the deposition hole perimeter and the boundary conditions, resulting in a computed Q_n value of zero. Therefore, a fine grid resolution is imperative for a robust and reliable numerical solution.

Additionally, the results suggest that implementing the hollow cylinder case introduce an artificial quantity of solute proportional to the size of the wall cell. This artificial solute is then transported to the surrounding cells, affecting flow rate measurement. Figure 2-3 shows that at Pe =50, the amount of artificial solute is negligible when the wall cell size is smaller than a few percent of the deposition hole radius, but becomes significant beyond that threshold, approximately 4.4 [mm] in this example. At higher Péclet numbers, such as 4018, the artificial solute becomes increasingly significant even for smaller wall cell sizes, larger that than 0.1 % times the deposition hole radius (Ferry, 2020c). Thus, careful selection of an appropriate wall cell size is recommended when implementing this approach to avoid introducing artificial solute and ensure accurate flow rate measurement.
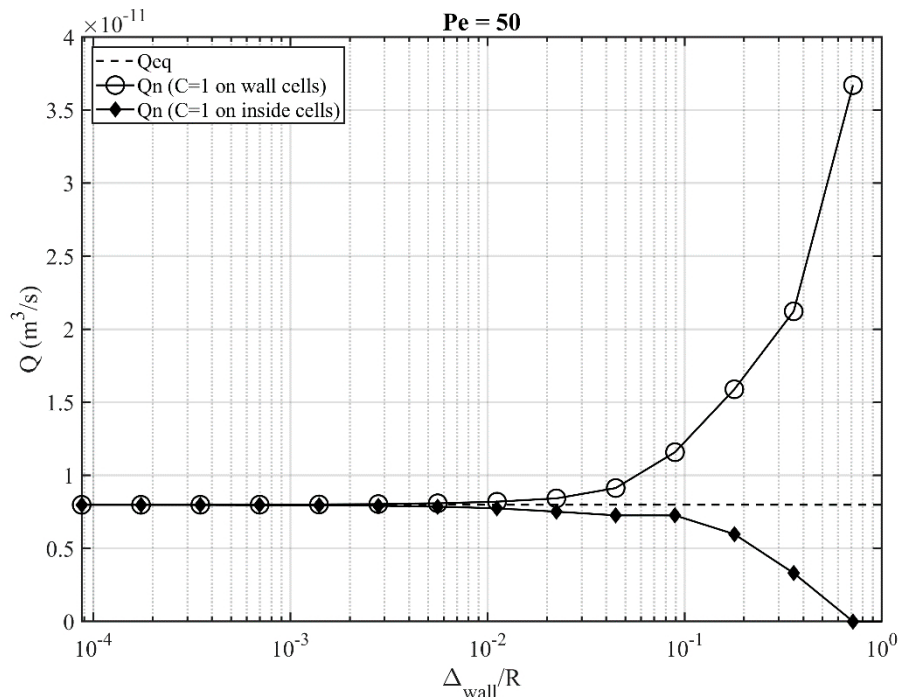

Figure 2-3. *Effect of wall cell size and boundary condition on the calculated flow rates, Q_{eq}.*

2.3   Effect of transport conditions, Péclet number

In addition, a comparative analysis is conducted to assess the performance of the Q_{eq} and Q_n, under varying transport conditions, specifically focusing on the Péclet numbers. To maintain consistency, the ratio of wall cell size[9] to radius, Δ_{wall}/R, is kept constant at 7×10^{-4} for all simulations. Figure 2-4 presents the results of this analysis, which align with the sensitivity analysis findings reported in (Ferry, 2020c).

Our analysis confirms that for an accurate estimation of Q_{eq}, the Péclet number must fall within the range of 4 to 700. Deviations from this range lead to significant discrepancies in Q_{eq} prediction due to the assumptions underlying the analytical formulation. When Péclet is less than 4, the Q_{eq} overestimates Q_n due to the absence of longitudinal transport (refer to Figure 2-5a), whereas for Péclet values greater than 700, Q_{eq} underestimates Q_n due to the brief contact time between flowing water and the deposition hole surface (as depicted in Figure 2-5 d).

These findings underscore the importance of selecting an appropriate Péclet number when using the Q_{eq} model in DarcyTools simulations to ensure accurate predictions of transport rate. It is worth noting that these conclusions are independent of the specific values of transmissivity, porosity, and effective diffusivity in the domain; they remain valid for the specified Péclet numbers.

Furthermore, Appendix D extends the Péclet number analysis to square and elliptical-shaped deposition holes. The results reveal that a similar range of Péclet values exists for which the Q_n and Q_{eq} align for these geometric configurations.
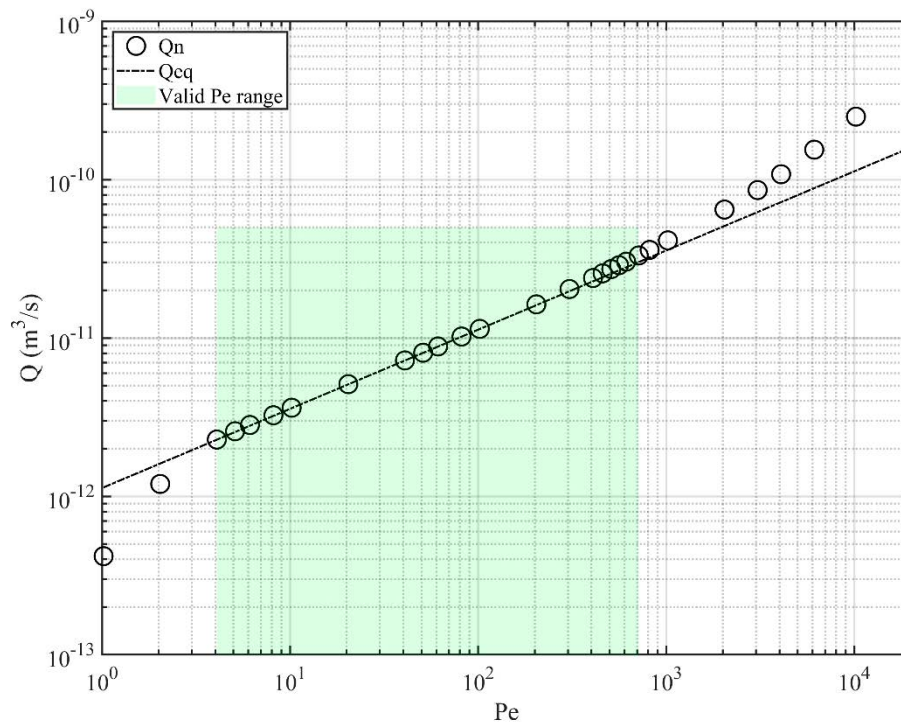
Figure 2-4. *Estimated Q_{eq} values at different Péclet numbers for a deposition hole with circular cross-section area. $\Delta_{wall}/R = 7 \times 10^{-4}$. The green zone indicates where the relative deviation between Q_n and Q_{eq} is less than 10 %.*

---

[9] In DarcyTools, grids are represented as lattices with Δx and Δy as grid spacings. In 2D, Δ_{wall} refer to $\Delta x = \Delta y$.
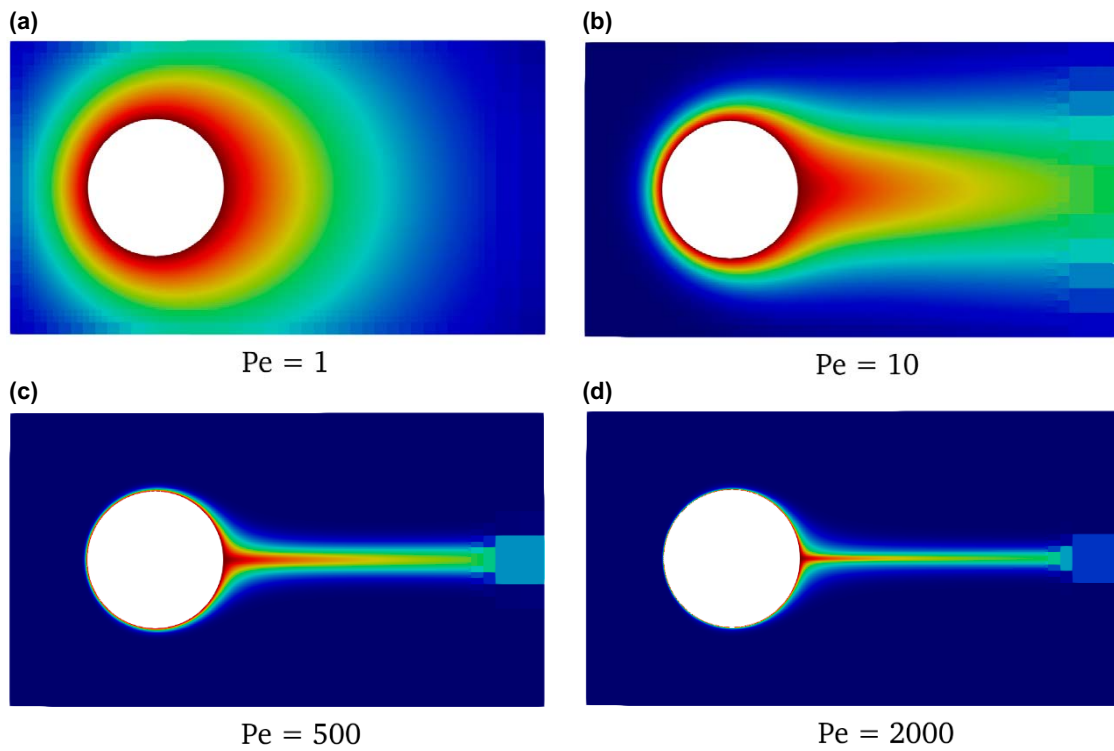
Figure 2-5. *Solute concentration profile around a deposition hole with circular cross-section area at different Péclet numbers.*

3 Investigation of the Q_{eq} model's efficacy in a 3D domain

3.1 Introduction and overview

The 2D model results have demonstrated that achieving a close match between Q_n value obtained through numerical integration and the analytically calculated Q_{eq} requires a fine mesh at the wall boundary of the deposition hole. For a cylindrical deposition hole with radius R, it has been found that the minimal difference can be attained with a wall cell size of $\Delta_{wall} = 5.0 \times 10^{-3} \times R$, for Pe = 50 (as depicted Figure 2-3) and $\Delta_{wall} = 2.8 \times 10^{-4} \times R$ for Pe = 4018 (Ferry, 2020c) when Pe falls within the range of 4 and 700. For a radius of $R = 0.875$ m, these required cell sizes translate to $\Delta_{wall} = 4.4$ [mm] and 0.25 [mm] for Pe = 50 and Pe = 4018, respectively. However, implementing such small cell sizes in realistic 3D repository-scale models is computationally expensive.

In contrast to the numerical integration approach, which demands a fine grid and significant computational resources, the semi-analytical formulation of Q_{eq} offers a computational advantage as it utilizes flow information to estimate solute transport without requiring a very fine grid or numerical integration. This alternative approach can be executed using a coarser mesh, making it a more efficient method for assessing Q_{eq} values in large-scale 3D models.

To build confidence in the application of the Q_{eq} model within DarcyTools, this section provides an in-depth investigation of the model's performance across various intersection scenarios, as outlined below:

1. A single fracture intersecting a deposition hole at a right angle.

2. Two parallel fractures intersecting a deposition hole at a right angle.

3. Single fracture intersecting a deposition hole at an angle.

4. Two fractures intersecting each other inside the deposition hole.

5. A single fracture with spatially variable conductivities and porosity intersecting a deposition hole at a right angle.

All test cases are conducted using DarcyTools version 4.2.37, and values of $Q_{eq\text{-}Numerical}$ and $Q_{eq\text{-}Semi\text{-}Analytical}$ are compared. In cases where applicable, $Q_{eq\text{-}Analytical}$ values are also computed using equivalent 2D models. It is important to note that in all scenarios, the fractures are assumed to be completely open and fully intersect with the deposition hole. The following sections provide detailed descriptions of each scenario and their corresponding results, thereby assessing the model's capacity to deliver accurate predictions across a range of intersection settings.

3.2 A single fracture intersecting a deposition hole at a right angle

In this scenario, flow and transport are simulated around a 3D deposition hole (DH) that is intersected by a single fracture at a right angle, as illustrated in Figure 1-8(a). In this scenario, our primary objective is to evaluate $Q_{eq\text{-}Semi\text{-}Analytical}$ with $Q_{eq\text{-}Numerical}$ by checking the influence of the deposition hole's cell size. We seek to determine the appropriate cell size within and surrounding the deposition hole, such that $Q_{eq\text{-}Semi\text{-}Analytical}$ equals $Q_{eq\text{-}Numerical}$.

Computational domain

The vertical deposition hole is created with height and radius of 8.2 m and 0.875 m, respectively. The horizontal fracture extends 50 m in x- and y-directions and has a thickness of 0.25 mm. The fracture transport properties are listed in Table 3-1. Centres of the domain boundary cells on east and west sides stand in −25 m and +25 m, respectively, while the y and z directions extend from −25 m to +25 m, independent of the cell size.

Pressure boundary condition

The pressure head gradient is specified as 0.01 m/m by fixing the pressure to 4 905 Pa at the centre of west cells and 0.0 Pa at the centre of east cells. The south, north, high, and low boundaries are no-flow boundary conditions.

Table 3-1. General flow and transport properties used in simulations.

Property	Value
DH radius, R, [m]	0.875
DH height, H, [m]	8.2
Fracture thickness, Δ, [mm]	0.25
Fracture porosity, ε, [-]	1.0
Fracture conductivity, k_1 [m/s]	5.71×10^{-6}
Water diffusivity, D_w, [m²/s]	1×10^{-9}
Head gradient, [m/m]	0.01
Péclet, Pe	50.0

3.2.1   Numerical framework

The $Q_{eq\text{-}Numerical}$ is computed by the solute transport integration technique, over a measurement box object that encloses the intersection zone. The box extends 0.5 m above and below the intersection zone and has a rectangular section with length and width of 6 m and 4 m, respectively, as shown in Figure 3-1.

Grid generation

The grid is constructed in several stages. The initial grid is built for the entire domain with a 5.0 m cell size. This is followed with a 0.01 m refinement in the area between the deposition hole and the measurement box, and a 0.001 m refinement at the edges of the deposition hole, which gives 0.61 mm wall cell size in x-, y- and z-directions, $\Delta_{wall}/R = 7 \times 10^{-4}$. The cell properties are then computed based on the properties of the known fracture. Finally, the non-conductive cells are removed. The refinement at the wall of the deposition hole is selected so that wall cells are small enough for an accurate solute transport integration, $Q_{eq\text{-}Numerical}$, on a cylinder with $R = 0.875$ m and at Pe = 50 (See Figure 2-3).
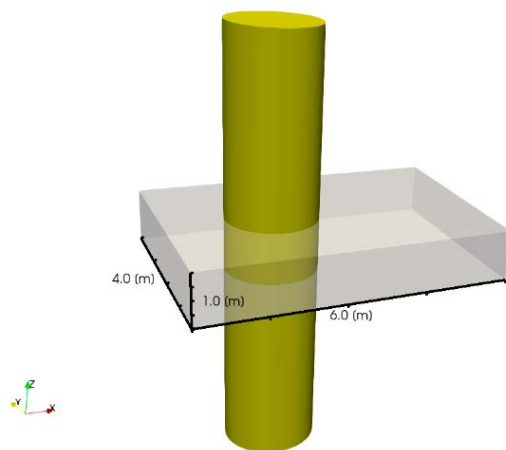

Figure 3-1. *Illustration of the measurement box (grey) used for capturing the rate of solute transported from deposition hole (yellow).*

Properties

In the numerical scheme, the remaining conductive cells (after removal of non-conductive cells) standing inside the deposition hole are forced to be non-conductive, similar to the "filled cylinder" case in the 2D study. Furthermore, a suggested pseudo-transient technique[10], which consists in setting a non-zero storativity and porosity in non-conductive cells is applied (Ferry, 2020c).

Concentration boundary condition

Concentration is set to C = 1 for cells standing inside the deposition hole, while the default no-flux concentration boundary conditions are set at the boundary of the domain.

$Q_{eq\text{-}numerical}$ calculation

The measurement box surrounding the deposition hole is used for integrating $Q_{eq\text{-}numerical}$. The solute flow rate is computed by the <flux> command with 'vfr' as the <type> argument, the concentration variable name 'C' as <cval> argument, and with <bycell> 'F'. The <loc> argument of the command <flux> is set to its default value, i.e., "all".

3.2.2   Semi-analytical framework

Grid generation

To improve computational efficiency compared to the $Q_{eq\text{-}Numerical}$, a coarser grid is constructed in the semi-analytical framework. The initial grid is built for the entire domain, with a 5.0 m cell size. This is followed with a 0.1 m refinement both at the edges of the deposition hole, and in the area between the deposition hole and the measurement box. This results in 0.078 m cell size inside and around the deposition hole, in x-, y- and z-directions. Furthermore, during the removal of the non-conductive cells, the cells standing inside and at the wall of the deposition hole are *not* removed. These cells are kept for the sake of estimating the U_M and θ_M, yet many of them are non-conductive.

Properties

The cell properties are computed based on the properties of the known fracture object. However, contrary to the $Q_{eq\text{-}Numerical}$, the cell standing inside the deposition hole are *not* forced to be non-conductive. The flow boundary conditions are not changed from the $Q_{eq\text{-}Numerical}$. It should also be emphasized that because we intend to use Equation (1-34) to estimate $Q_{eq\text{-}Semi\text{-}Analytical}$, it is not necessary to solve the solute transport equation for this problem.

$Q_{eq\text{-}Semi\text{-}Analytical}$ calculation

The $Q_{eq\text{-}Semi\text{-}Analytical}$ is computed using the flow information and Equation (1-34). U_M, can be computed via Equation (1-36) using the net flow values in x-, y- and z- directions, Equations (1-37) to (1-39)[11]. The corresponding <loc> argument gathers the cells standing inside and at the border of the deposition hole. The mean porosity, θ_M, is estimated by a built-in user function[12] on the same location, see Equation (1-35). For a sample implementation of the process described above in DarcyTools, please refer to the CIF and FIF file examples provided in Appendix E.

---

[10] The pseudo-transient technique is a trick to enhance the efficiency of the solvers. It is particularly useful in cases where residual non-conductive cells exist in the computational domain, for example, after a cell removal operation.

[11] Provided by the <flux> command with the <type> argument 'vfl' in DarcyTools.

[12] GET_VAR_MEAN

3.2.3 Cell size study

Since the estimations of U_M and θ_M are sensitive to the fracture cell size as well as the sizes of the cells standing inside and at the border of the deposition hole, while we keep these cell sizes equal, we vary them to study their size effect on the $Q_{eq\text{-}Semi\text{-}Analytical}$ results, at Pe = 50. The results, as shown in Figure 3-2, suggest that as the cell size reduces, the difference between $Q_{eq\text{-}Semi\text{-}Analytical}$ and $Q_{eq\text{-}Numerical}$ reduces and tends toward a limit. With a Pe value of 50, a cell size of 0.078 m and a Δ_{wall}/R ratio of 0.09 can provide a reliable estimation of $Q_{eq\text{-}Numerical}$. Notably, this cell size is not excessively small, and it can be applied in realistic 3D repository cases. Therefore, this refinement is utilized in subsequent 3D studies to estimate $Q_{eq\text{-}Semi\text{-}Analytical}$ in various intersection scenarios.

3.2.4 Parameter study

We also run a parameter study for the single fracture model, in which the three Q_{eq} values are estimated for increasing values of fracture conductivity in Case 1A with $k = k_1$, Case 1B with $k = 5 \times k_1$ and Case 1C with $k = 10 \times k_1$. The reader may note in this specific scenario where a single horizontal fracture intersects a vertical deposition hole, it is possible to estimate the analytical equivalent flow rate, denoted as Q_{eq} by using a two-dimensional model similar to the one presented in Chapter 2. This involves incorporating the flow information obtained from the numerical setup mentioned above in Section 3.2.1.

The results, summarized in Table 3-2, show good agreement between $Q_{eq\text{-}Semi\text{-}Analytical}$ and $Q_{eq\text{-}Numerical}$. It can also be seen that the $Q_{eq\text{-}Analytical}$ and $Q_{eq\text{-}Semi\text{-}Analytical}$ values in Case 1B and Case 1C are $\sqrt{5}$ and $\sqrt{10}$ times larger than those in Case 1A, respectively. This is expected from Equation (1-21) and the linear dependence of Darcy flux on the fracture conductivity.

Table 3-2. Transport parameters and Q_{eq} results for a single fracture for Pe = 50, 250, 500.

Parameter	Case 1A, k = k₁	Case 1B, k = 5×k₁	Case 1C, k = 10×k₁
Fracture aperture[13], b_f, [mm]	0.25	0.25	0.25
Head gradient, h, [m/m]	0.01	0.01	0.01
Fracture conductivity, k, [m/s]	**5.71E−6**	**2.86E−5**	**5.71E−5**
Péclet	**50**	**250**	**500**
$Q_{eq\text{-}Numerical}$, [m³/s]	7.96E−12	1.79E−11	2.60E−11
$Q_{eq\text{-}2D\text{-}Analytical}$, Q_{eq}, [m³/s]	7.98E−12	1.78E−11	2.52E−11
$Q_{eq\text{-}Semi\text{-}Analytical}$, [m³/s]	7.91E−12	1.77E−11	2.50E−11
θ_M, [-]	3.02E−05	3.02E−05	3.02E−05
U_M, [m/s][14]	1.73E−12	8.65E−12	1.73E−11
$\theta_M \times U_M$, [m/s]	5.23E−17	2.61E−16	5.22E−16

---

[13] Mechanical aperture

[14] In this case, $U_M = \theta_M U_{d,f}$, where $U_{d,f} = k \times h$.

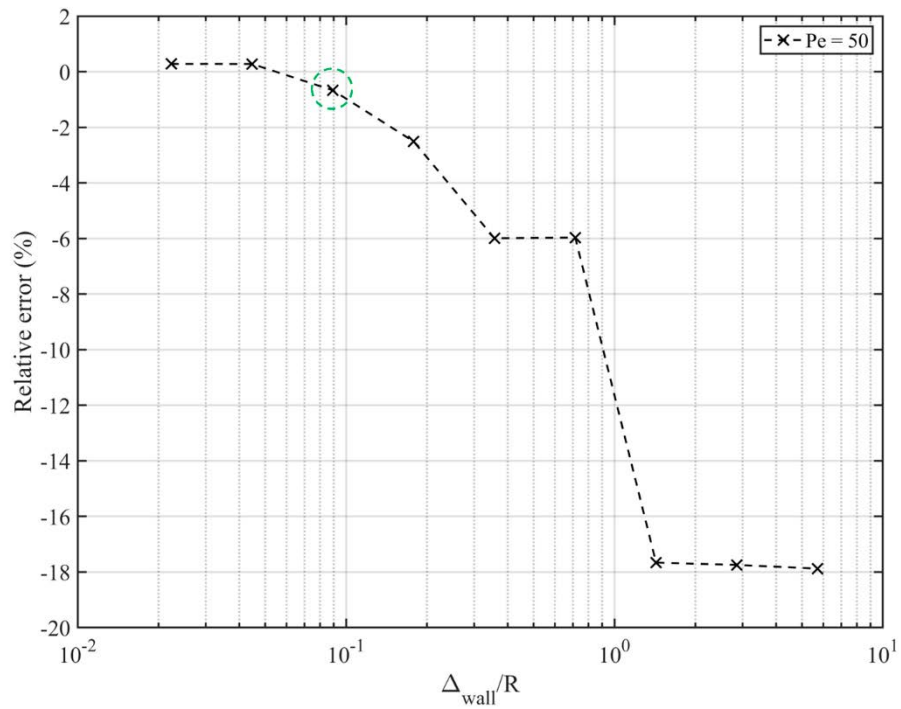**Figure 3-2.** *The relative difference between $Q_{eq\text{-}Semi\text{-}Analytical}$ and $Q_{eq\text{-}Numerical}$ as a function of cell size in and around the deposition hole. The highlighted point, denoted by a green circle represents the chosen wall cell size.*
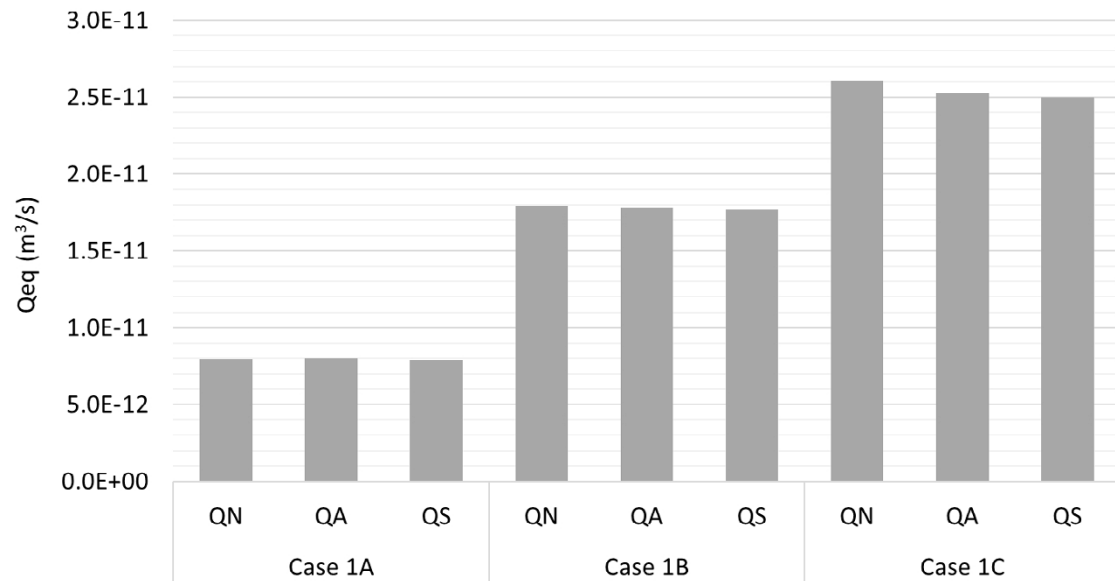

Figure 3-3. *QN, QA, QS denote $Q_{eq\text{-}Numerical}$, $Q_{eq\text{-}2D\text{-}Analytical}$ and $Q_{eq\text{-}Semi\text{-}Analytical}$, respectively.*

3.3 Two parallel fractures intersecting a deposition hole at a right angle

In this scenario, flow and transport are simulated around a vertical 3D deposition hole that is intersected by two fractures at a right angle, as shown in Figure 3-4. The spacing between the fractures is 1.0 m. We study three cases, namely Case 2A, 2B and 2C, where the hydraulic conductivity of the second fracture is 1, 5 and 10 times larger than the reference fracture, as defined in Case 1A. Given the numerical and semi-analytical frameworks discussed in Sections 3.2.1 and 3.2.2, the Q_{eq} values for this system are obtained and the following equations are investigated. Transport parameters of the 2nd fracture, Q_{eq} results, and relative errors for the three cases are listed in Table 3-3.

$$\epsilon_1 = \frac{Q_{eq-Numerical} - Q_{eq-Analytical}}{Q_{eq-Analytical}} \quad \left(Q_{eq-Analytical} = Q_{eq}\big|_{1,Circle} + Q_{eq}\big|_{2,Circle}\right) \qquad (3\text{-}1)$$

$$\epsilon_2 = \frac{Q_{eq-Semi-Analytical} - Q_{eq-Numerical}}{Q_{eq-Numerical}} \qquad (3\text{-}2)$$

The results indicate that the $Q_{eq\text{-}Semi\text{-}Analytical}$ estimations in this scenario are in good agreement with $Q_{eq\text{-}Numerical}$ values. As observed, the relative error in Equation (3-1) increases when the conductivity, represented by the Péclet number, is elevated in the second fracture. This result aligns with the conclusions presented in Figure 2-4, which indicates that an increase in the Péclet number leads to a rise in the relative error between $Q_{eq\text{-}Numerical}$ and Q_{eq}. This correlation can be attributed to the fact that a higher Péclet number signifies a more pronounced advection-dominated transport, which can cause a deviation from the assumptions underlying the analytical model used to estimate Q_{eq}.

Table 3-3. Transport parameters of the 2nd fracture and results for the parallel fractures system.

| Parameter/Value	Case 2A, $k_2 = k_1$	Case 2B, $k_2 = 5 \times k_1$	Case 2C, $k_2 = 10 \times k_1$
Fracture aperture, b_f, [mm]	0.25	0.25	0.25
Head gradient, h, [m/m]	0.01	0.01	0.01
2nd Fracture conductivity, k, [m/s]	**5.71E−6**	**2.86E−5**	**5.71E−5**
$Q_{eq\text{-}Numerical}$, [m³/s]	1.60E−11	2.60E−11	3.41E−11
$Q_{eq1} + Q_{eq2}$ [m³/s]	1.60E−11	2.58E−11	3.32E−11
$Q_{eq\text{-}Semi\text{-}Analytical}$, [m³/s]	1.58E−11	2.74E−11	3.70E−11
θ_M, [-]	6.04E−05	6.04E−05	6.04E−05
U_M, [m/s]	3.46E−12	1.04E−11	1.90E−11
$\theta_M \times U_M$, [m/s]	2.09E−16	6.26E−16	1.15E−15
Relative error, ϵ_1, (%)	−0.06	0.57	2.70
Relative error, ϵ_2, (%)	−0.93	5.36	8.61
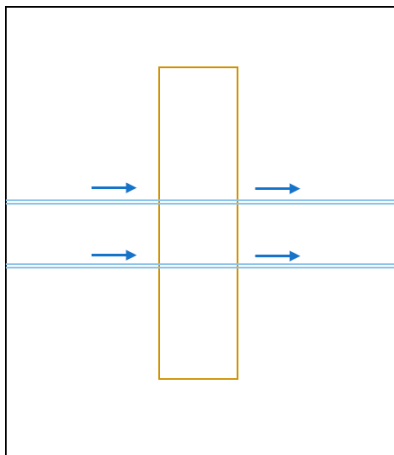
Figure 3-4. *Illustration of two parallel fractures intersecting a deposition hole at a right angle.*
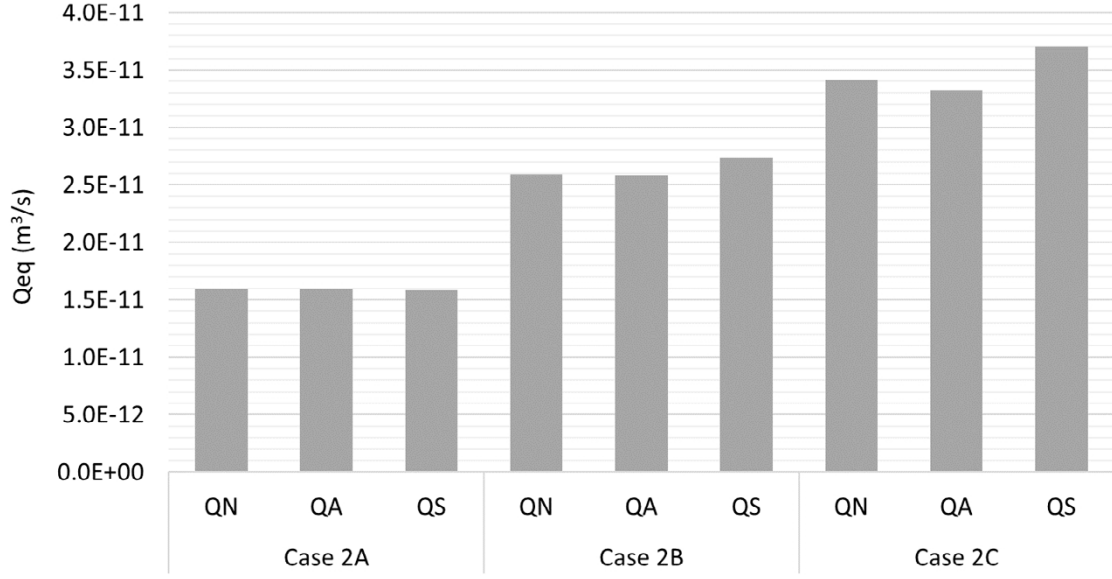
Figure 3-5. *QN, QA, QS denote $Q_{eq\text{-}Numerical}$, $Q_{eq\text{-}2D\text{-}Analytical}$ and $Q_{eq\text{-}Semi\text{-}Analytical}$, respectively.*

The reader may note that the three Q_{eq} values in Case 2A are twice larger than their corresponding values in Case 1A. This is expected as the transport capacity of the system is now doubled by introducing the second identical fracture. Similarly, the reader may also note that increasing the conductivity of the 2nd fracture in Cases 2B and 2C by 5 and 10 times causes the $Q_{eq\text{-}Analytical}$ values to, respectively, increase by factors $(1+\sqrt{5})$ and $(1+\sqrt{10})$, relative to the $Q_{eq\text{-}Analytical}$ value in Case 1A. This is also expected given the $Q_{eq\text{-}Analytical}$ formulation, Equation (1-21)

It can also be seen that $Q_{eq\text{-}Semi\text{-}Analytical}$ value in Case 2B is $\sqrt{2 \times (1+5)}$ times larger than that in Case 1A and the one of Case 2C is $\sqrt{2 \times (1+10)}$ times larger than that in Case 1A. This is also expected given the $Q_{eq\text{-}Semi\text{-}Analytical}$ formulation, Equation (1-34). In general, in this scenario where two parallel fractures with similar aperture intersect the deposition hole at a right angle, and $k_2 = \beta \times k_1$, θ_M can be expressed as:

$$\theta_M = 2\frac{b_f}{H} \tag{3-3}$$

and DarcyTools calculates U_M through the following calculation:

$$U_M = \frac{b_f}{H}(1+\beta)U_{d,f} \tag{3-4}$$

Hence $Q_{eq\text{-}Semi\text{-}Analytical}$ expression gives:

$$Q_{eq-Semi-Analytical} = 8b_f\sqrt{\frac{D_w R}{\pi}}\sqrt{2 \times (1+\beta)U_{d,f}} \tag{3-5}$$

3.4 Single fracture intersecting a deposition hole at an angle

Objectives in this scenario are similar to those in Section 3.2. The only exception is that flow and transport are simulated around a vertical deposition hole that is intersected by a fracture at an angle. This is illustrated in Figure 3-6. We study three cases, namely, Case 3A, 3B and 3C, where the inter-section angle, α, is, respectively, 60°, 45° and 30°. In all the cases, it is assumed that the fracture fully intersects the deposition hole.
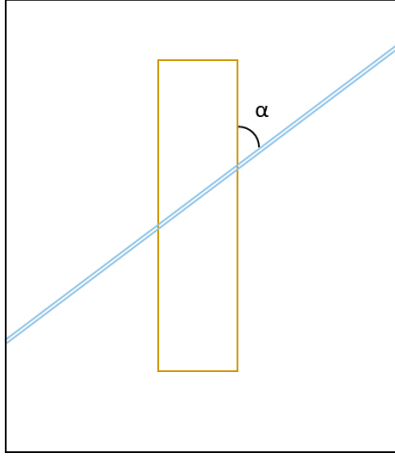
Figure 3-6. *Illustration of a single fracture intersecting a deposition hole at an angle.*

The analytical Q_{eq} for these inclined fractures are estimated using Equation (1-21) and flow information from 2D models with elliptical intersection area and with similar transport conditions to their associated 3D models. $Q_{eq\text{-}Numerical}$ and $Q_{eq\text{-}Semi\text{-}Analytical}$ are estimated using the numerical and semi-analytical frameworks discussed in Sections 3.2.1 to 3.2.2. The resulted Q_{eq} values for the three cases are found and the following equations are investigated.

$$\epsilon_1 = \frac{Q_{eq-Numerical} - Q_{eq}\big|_{\text{ellipses}}}{Q_{eqh}\big|_{\text{ellipses}}} \tag{3-6}$$

$$\epsilon_2 = \frac{Q_{eq-Semi-Analytical} - Q_{eq-Numerical}}{Q_{eq-Numerical}} \tag{3-7}$$

Case	Concentration (3D View)	Concentration (2D View)
Case 3A α=60⁰		
Case 3B α=45⁰		
Case 3C α=30⁰		

Figure 3-7. *Concentration distributions in the single fracture intersecting the deposition hole at different angles.*

The study's findings are summarized in Table 3-4, indicating that $Q_{eq\text{-}Numerical}$ provides close estimates to Q_{eq} (obtained from the 2D models) for all three cases, as expected. However, achieving this level of accuracy comes at a high computation cost. On the other hand, $Q_{eq\text{-}Semi\text{-}Analytical}$ values demonstrate good agreement wi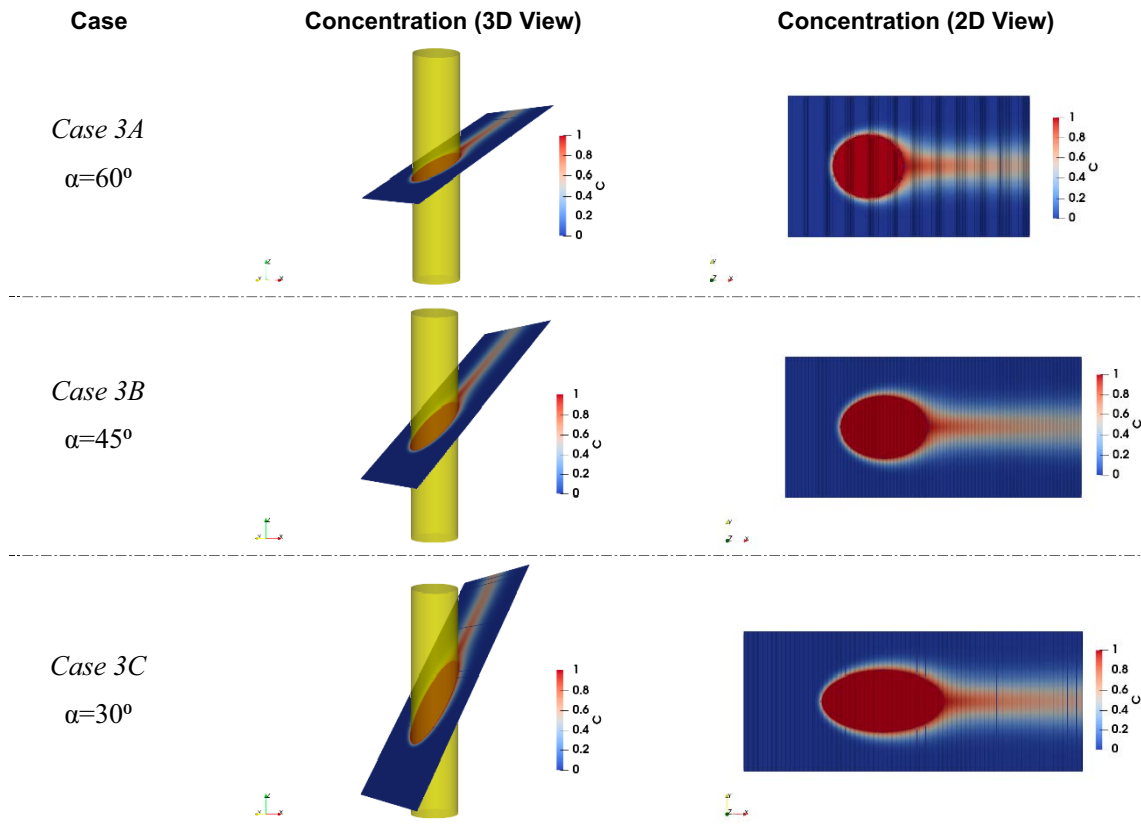th the Q_{eq} results, particularly for intersection angles ranging between $45° < α < 90°$. Nevertheless, it noteworthy that as the intersection angle decreases, the relative error in Equation (3-7) increases, reaching a maximum of 13.7 % at α=30°.

Table 3-4. Results for the single fracture intersecting the deposition hole at different angles.

Fracture Property	Case 3A	Case 3B	Case 3C
Fracture aperture, b_f, [mm]	0.25	0.25	0.25
Head gradient, h, [m/m]	0.012	0.014	0.020
Fracture conductivity, k, [m/s]	5.71E−6	5.71E−6	5.71E−6
Intersection angle, α	**60°**	**45°**	**30°**
$Q_{eq\text{-}Numerical}$, [m³/s]	8.31E−12	9.17E−12	1.01E−11
Q_{eq}, [m³/s]	8.27E−12	8.70E−12	9.49E−12
$Q_{eq\text{-}Semi\text{-}Analytical}$, [m³/s]	8.33E−12	9.78E−12	1.15E−11
$θ_M$, [-]	3.49E−05	4.27E−05	6.04E−05
U_M, [m/s]	1.66E−12	1.87E−12	1.83E−12
$θ_M × U_M$, [m/s]	5.80E−17	8.00E−17	1.11E−16
$ε_1$ in Equation (3-6), (%)	0.4	5.35	6.74
$ε_2$ in Equation (3-7), (%)	0.32	6.69	13.68
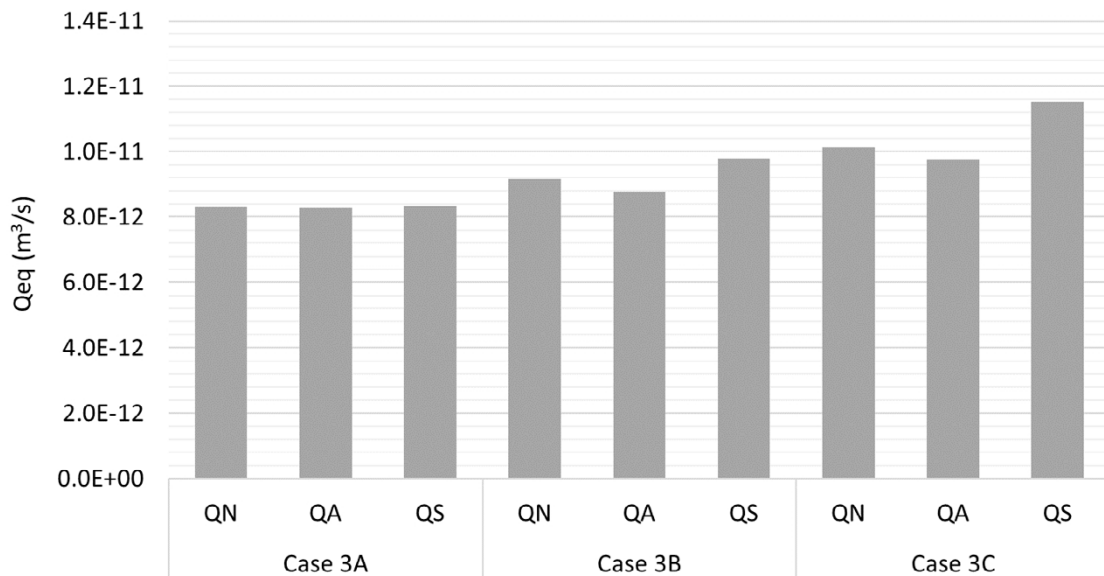
Figure 3-8. *QN, QA, QS denote $Q_{eq\text{-}Numerical}$, $Q_{eq\text{-}2D\text{-}Analytical}$ and $Q_{eq\text{-}Semi\text{-}Analytical}$, respectively.*

3.5 Two fractures intersecting each other inside the deposition hole

In this scenario, flow and transport are simulated around a 3D deposition hole that is fully intersected by two fractures at different angles, as shown in Figure 3-9. Note that none of the fractures in this case reach the two faces of the domain where the pressure is fixed. Thus, flow enters by one fracture and leave by another one and, therefore, only part of fracture 1 and part of fracture 2 contribute to the solute diffusion. We study three cases where the hydraulic conductivity of the second fracture is 1, 5, and 10 times larger than the reference fracture, k_1, with $\alpha_1 = \alpha_2 = 60°$. We investigate how $Q_{eq\text{-}Semi\text{-}Analytical}$ compares to the $Q_{eq\text{-}Numerical}$, Equation (3-8). Note that no easy way could be found to estimate the analytical solution $Q_{eq\text{-}Analytical}$ for these cases. The results are summarized in Table 3-5.

$$\epsilon_2 = \frac{Q_{eq-Semi-Analytical} - Q_{eq-Numerical}}{Q_{eq-Numerical}} \tag{3-8}$$

The $Q_{eq\text{-}Numerical}$ result in Case 4A (for identical fractures) is comparable to the $Q_{eq\text{-}Numerical}$ value in Case 3A. This is expected due to the symmetry of the fractures. That is, half of the fracture 1 and half of the fracture 2 contribute to the solute transport. On the other hand, $Q_{eq\text{-}Semi\text{-}Analytical}$ overestimates $Q_{eq\text{-}Numerical}$ in this scenario, and the relative error in Equation (3-8) is generally high, ranging from 21.8 % (for $k_2 = 10 \times k_1$) to 27.5 % for ($k_2 = k_1$). The difference between $Q_{eq\text{-}Numerical}$ and $Q_{eq\text{-}Semi\text{-}Analytical}$ comes from the fact that during calculation of the $Q_{eq\text{-}Semi\text{-}Analytical}$, volumes of the dead-end parts of the fractures contribute to the mean porosity value, θ_M, via Equation (1-35). However, in practice, the dead-end parts do not participate in the transport of solute.
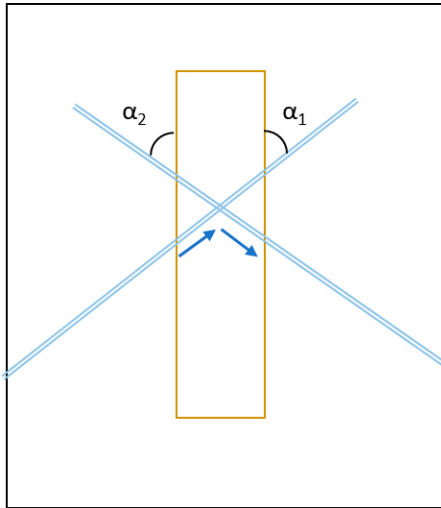
Figure 3-9. *Illustration of two fractures with different transmissivities intersecting each other inside the deposition hole.*
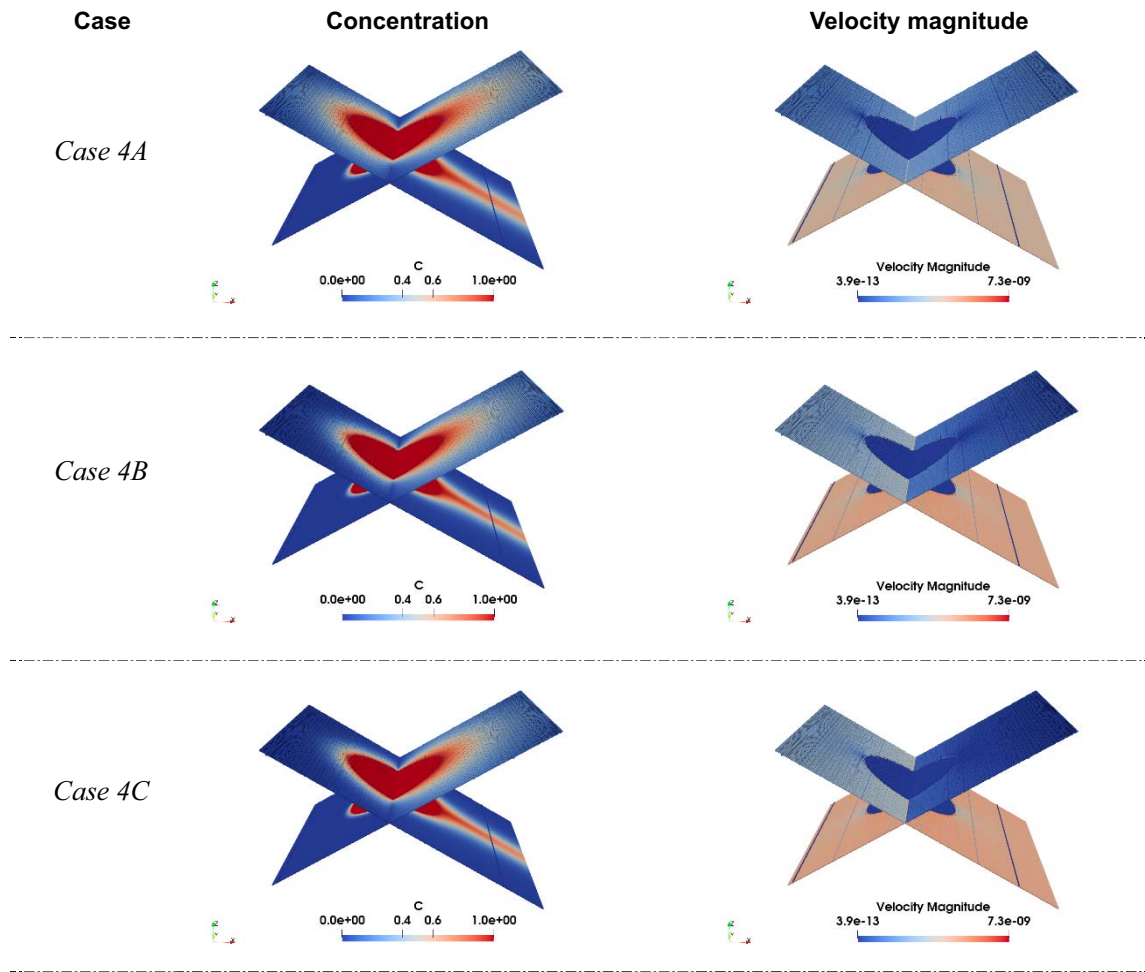
Figure 3-10. Concentration and velocity distributions of the two fractures with different transmissivities intersecting each other inside the deposition hole.

Table 3-5 Transport parameters and results for the two fractures with different transmissivities intersecting each other inside the deposition hole.

Fracture Property	Case 4A, $k_2 = k_1$	Case 4B, $k_2 = 5 \times k_1$	Case 4C, $k_2 = 10 \times k_1$
Fracture aperture, b_f, [mm]	0.25	0.25	0.25
Head gradient, h, [m/m]	0.012	0.014	0.020
2nd Fracture conductivity, k, [m/s]	**5.71E−6**	**2.86E−5**	**5.71E−5**
$Q_{eq\text{-}Numerical}$, [m^3/s]	8.59E−12	1.17E−11	1.23E−11
$Q_{eq\text{-}Semi\text{-}Analytical}$, [m^3/s]	1.10E−11	1.43E−11	1.50E−11
θ_M, [-]	18.1	30.8	33.9
U_M, [m/s]	6.97E−05	6.97E−05	6.97E−05
$\theta_M \times U_M$, [m/s]	1.44E−12	2.45E−12	2.70E−12
ϵ_2 in Equation (3-8), (%)	27.52	22.60	21.88
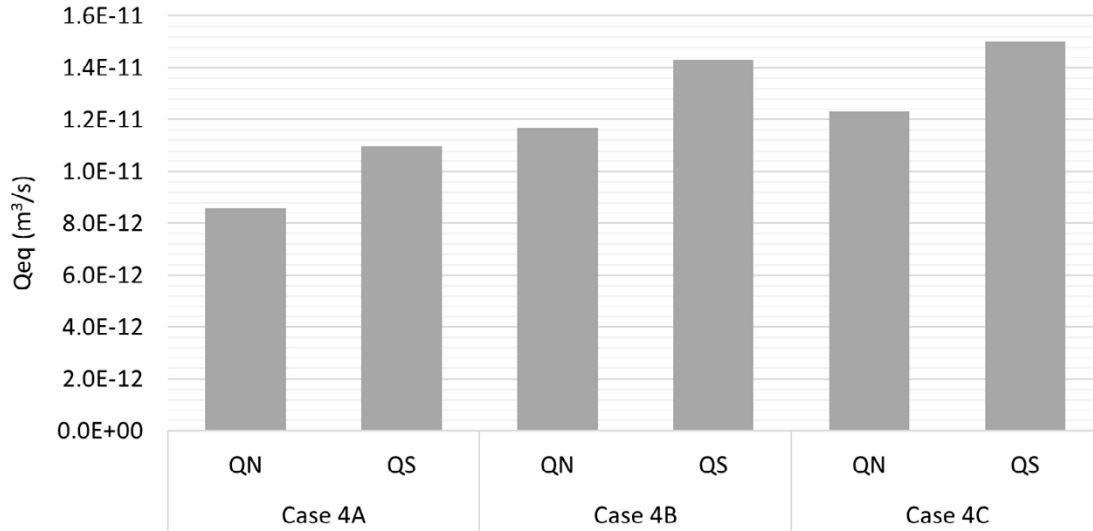
Figure 3-11. ***QN, QS*** *denote $Q_{eq\text{-}Numerical}$ and $Q_{eq\text{-}Semi\text{-}Analytical}$, respectively.*

3.6   A single fracture with spatially variable properties

In this scenario, we study flow and transport in a similar system described in Section 3.2, i.e., a fracture fully intersecting the deposition hole at a right angle. The only exception is that now we introduce a fracture with spatially variable transport properties, i.e., conductivity and porosity.

Questions of interest in this scenario are:

How does $Q_{eq\text{-}Semi\text{-}Analytical}$ compare to the $Q_{eq\text{-}Numerical}$?

How does $Q_{eq\text{-}Semi\text{-}Analytical}$ compare to its corresponding value in a smooth parallel plate fracture with uniform properties?

The above questions are investigated for different realizations of the fracture with stochastic porosity and conductivity values. In DarcyTools, this property variability can be introduced by using the "inhomogeneous" feature of a known fracture command <knwf> (Ferry, M., 2020a). We investigate the accuracy of the following equations:

$$\epsilon_2 = \frac{Q_{eq-Semi-Analytical} - Q_{eq-Numerical}}{Q_{eq-Numerical}} \tag{3-9}$$

$$\epsilon_3 = \frac{Q_{eq-Semi-Analytical} - Q_{eq-Numerical}\big|_{Homogeneous, fracture}}{Q_{eq-Numerical}\big|_{Homogeneous, fracture}} \tag{3-10}$$

$$\epsilon_4 = \frac{Q_{eq-Numerical} - Q_{eq-Numerical}\big|_{Homogeneous, fracture}}{Q_{eq-Numerical}\big|_{Homogeneous, fracture}} \tag{3-11}$$

The simulation results are summarized in Table 3-6. The results indicate that by increasing the inhomogeneity level, both in terms of increasing the standard deviation in porosity and conductivity, and by reducing the correlation length, the relative errors in Equations (3-9) and (3-10) increase. In the studied cases, the observed differences between $Q_{eq\text{-}Numerical}$ and $Q_{eq\text{-}Semi\text{-}Analytical}$ in Equations (3-9) ranges between −0.54 % (for a small level of heterogeneity) to 28.8 % (for a greater level of heterogeneity).

The difference between $Q_{eq\text{-}Numerical}$ (for homogeneous fracture) and $Q_{eq\text{-}Semi\text{-}Analytical}$ (Equation (3-10)) follows a similar pattern, but the error is generally of larger magnitude, i.e., up to 48.6 %. Finally, it is shown that if an inhomogeneous fracture is treated as a homogeneous fracture with uniform mean properties[15], the maximum relative error in estimating $Q_{eq\text{-}Numerical}$ becomes 18.6 % in the studied cases. Please note that only one "fracture realization" is made for each case. To improve the reliability of the results, more realizations should be considered to confirm the results and to exclude the influence of random artefacts.

Table 3-6. Transport parameters and results for a single inhomogeneous fracture.

Parameter/Value	Case 1A	Case 5A	Case 5B	Case 5C	Case 5A_2	Case 5A_3
Fracture thickness, Δ, [mm]	0.25	0.25	0.25	0.25	0.25	0.25
Mean porosity	1.0	1.0	1.0	1.0	1.0	1.0
Mean conductivity, [m/s]	5.71E−6	5.71E−6	5.71E−6	5.71E−6	5.71E−6	5.71E−6
STDV (porosity & conductivity)	0.0	**1.0**	**0.5**	**0.1**	**1.0**	**1.0**
Correlation length (x- and y-direction)	0.0	**0.1**	**0.1**	**0.1**	**0.001**	**0.0001**
$Q_{eq\text{-}Numerical}$, [m^3/s]	7.96E−12	8.21E−12	7.79E−12	7.88E−12	9.44E−12	9.18E−12
$Q_{eq\text{-}Semi\text{-}Analytical}$, [m^3/s]	7.91E−12	9.74E−12	8.10E−12	7.84E−12	1.12E−11	1.18E−11
θ_M, [-]	3.02E−05	4.11E−05	3.16E−05	3.00E−05	4.60E−05	4.85E−05
U_M, [m/s]	1.73E−12	1.93E−12	1.74E−12	1.72E−12	2.27E−12	2.41E−12
$\theta_M \times U_M$, [m/s]	5.23E−17	7.94E−17	5.48E−17	5.14E−17	1.05E−16	1.17E−16
ϵ_2 in Equation (3-9), (%)	−0.67	18.74	3.99	−0.54	18.47	28.80
ϵ_3 in Equation (3-10), (%)	−0.67	22.41	1.75	−1.50	40.54	48.57
ϵ_4 in Equation (3-11), (%)	0.0	3.09	−2.16	−0.97	18.63	15.35
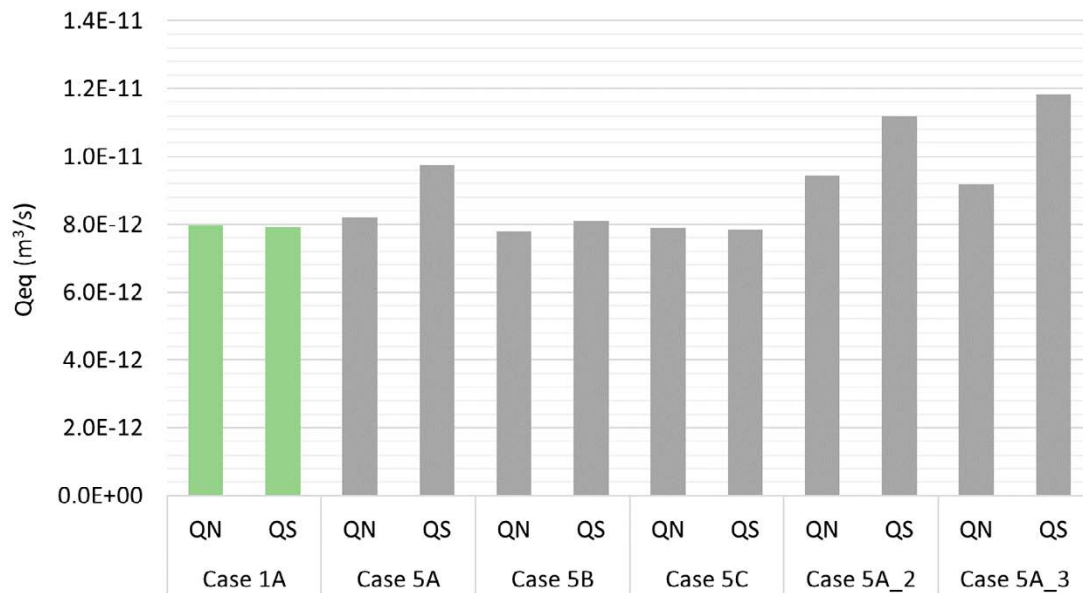
Figure 3-12. QN, QS denote $Q_{eq\text{-}Numerical}$ and $Q_{eq\text{-}Semi\text{-}Analytical}$, respectively.

---

[15] It is possible that the effective homogeneous aperture differs from the mean aperture.
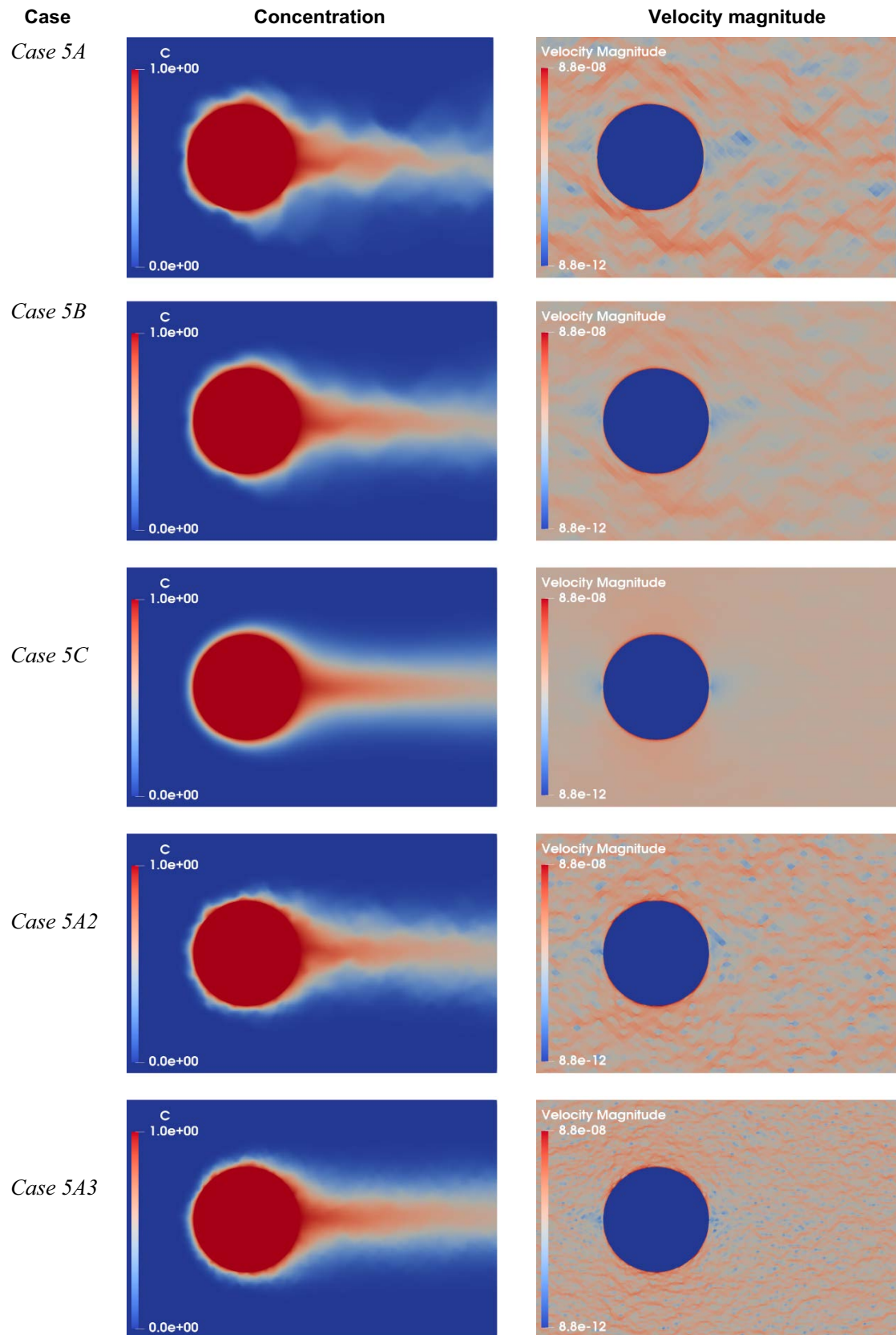
Figure 3-13. *Concentration and velocity distributions in a single fracture with inhomogeneous properties.*

3.7   Key Observations and Implications

This research focused on assessing the effectiveness of the $Q_{eq\text{-}Semi\text{-}Analytical}$ estimation in predicting $Q_{eq\text{-}Numerical}$, which closely approximate the actual Q_{eq}, across various intersection scenarios and fracture properties. The study findings can be summarized as follows:

1. **Singular or Parallel Homogeneous Fractures at Right Angles:** The $Q_{eq\text{-}Semi\text{-}Analytical}$ estimation demonstrated a high degree of accuracy in predicting $Q_{eq\text{-}Numerical}$ in scenarios involving singular or parallel homogeneous fractures that intersected the deposition hole at a right angle. The maximum relative error encountered during the investigation was 8.6 % for the parallel fracture case, indicating the reliability and robustness of this method in such situations.

2. **Non-Perpendicular Intersection Angles:** In cases where a single homogeneous fracture intersected the deposition hole at a non-perpendicular angle, the $Q_{eq\text{-}Semi\text{-}Analytical}$ estimations showed satisfactory agreement with $Q_{eq\text{-}Numerical}$. However, as the intersection angle (α) decreased, the relative error increased. A 13.7 % error was observed for $\alpha = 30°$ emphasizing the need for caution when employing this estimation method in scenarios with non-perpendicular intersection angles.

3. **Complex Intersection Scenarios with Different Transmissivities:** In more complex situations involving the intersection of two homogeneous fractures with different transmissivities within the deposition hole, the $Q_{eq\text{-}Semi\text{-}Analytical}$ estimations generally yielded higher values than $Q_{eq\text{-}Numerical}$, with a maximum error of 25.5 % in the cases examined. This suggests that extra caution should be exercised when using this method in complex intersection scenarios, as the potential for error is greater. Further research may be required to develop more accurate estimation methods for such cases.

4. **Nonhomogeneous Fractures:** For nonhomogeneous fractures, the study showed that as the level of inhomogeneity in a fracture increased, the differences between $Q_{eq\text{-}Semi\text{-}Analytical}$ and $Q_{eq\text{-}Numerical}$ also increased, as well as the difference between $Q_{eq\text{-}Semi\text{-}Analytical}$ and $Q_{eq\text{-}Numerical}$ for the associated homogeneous fracture. Maximum errors observed were 28.8 % and 48.6 %, respectively. Furthermore, treating an inhomogeneous fracture as a homogeneous one resulted in a maximum relative error of 18.6 % in estimating $Q_{eq\text{-}Numerical}$. It's important to note that these results were based on a single realization of the fracture in each case, and in practical applications, generating a sufficient number of realizations may reduce statistical errors in estimating $Q_{eq\text{-}Numerical}$.

The observed errors in the $Q_{eq\text{-}Semi\text{-}Analytical}$ estimation can be attributed to the approximation of $Q_{eq\text{-}ECPM}$ in Equation (1-32), specifically in the treatment of $\left(\sqrt{\theta U}\right)_{M-ECPM}$ as $\sqrt{\theta_M U_M}$. Accurate calculation of $Q_{eq\text{-}ECPM}$ necessitates the calculation of the mean value of the square root of θU, $\left(\sqrt{\theta U}\right)_{M-ECPM}$, for all cells inside and around the deposition hole to correctly represent the underlying fracture network. This was demonstrated in Section 3.5, where the dead-end parts of the fractures did not participate in solute transport, yet their volumes contributed to the mean porosity value, resulting in relatively larger values compared to $Q_{eq\text{-}Numerical}$. Similar explanations can apply to the errors observed in other scenarios.

While the authors currently could not identify a more reliable and generalizable alternative solution for calculating the mean value $\left(\sqrt{\theta U}\right)_{M-ECPM}$ based on the information provided by the ECPM methods in DarcyTools, it is crucial to note that the observed level of error in $Q_{eq\text{-}Semi\text{-}Analytical}$ is reasonable in comparison to the fundamental assumptions underlying the Q_{eq} model. For example, if only half of the deposition hole is intersected by the fracture, as depicted in Figure 3-14 (middle), $Q_{eq\text{-}Analytical}$ will be 100 % larger than the effective value ($Q_{eq\text{-}Numerical}$), as the Q_{eq} model assumes both sides of the deposition hole are in contact with flowing water. Similarly, if the fracture intersects only a quarter of the deposition hole, as depicted in Figure 3-14 (right), $Q_{eq\text{-}Analytical}$ will be approximately 180 % larger than the effective value ($Q_{eq\text{-}Numerical}$).
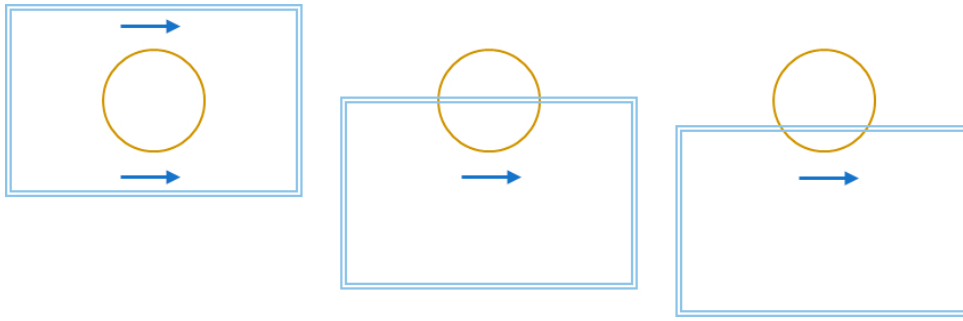
Figure 3-14. *Schematics of a fracture fully (left) and partially (middle and right) intersecting the deposition hole.*

Furthermore, considering the overestimation inherent in the semi-analytical approach discussed in this study, $Q_{eq\text{-}Semi\text{-}Analytical}$ can be considered a conservative estimate. It can serve as a preliminary estimation to assess the potential for contaminant transport from a block of rock containing a future deposition hole. In cases where problematic deposition holes are identified, the more computationally intensive $Q_{eq\text{-}Numerical}$ method can be employed as a secondary step.

In conclusion, the findings from this study offer insights into the limitations and applicability of the $Q_{eq\text{-}Semi\text{-}Analytical}$ estimation method. Researchers and DarcyTools users can utilize this information to make informed decisions regarding its use in various geological and hydrogeological scenarios, considering the level of accuracy required and computational resources available.

4 Q_{eq} model implementation in a large-scale repository model

The present study employs DarcyTools to model flow and transport in a simplified repository system comprising a fractured bedrock and fifty (50) deposition holes. The primary objectives are to demonstrate the implementation of the Q_{eq} model in a large scale DarcyTools model and to assess the effectiveness of the $Q_{eq\text{-}Semi\text{-}Analytical}$ approach for estimating the rates of solute transport. This will be achieved through a comparative analysis of $Q_{eq\text{-}Semi\text{-}Analytical}$ values with a) $Q_{eq\text{-}Numerical}$ values, which are obtained using the integration method, and b) Q_{eq} values derived from a Discrete Fracture Network (DFN) model in ConnectFlow.

It should be noted that the Q_{eq} values obtained from the DFN modelling were provided by SKB, as this modelling approach was not included in the scope of the current modelling effort presented in this report. These Q_{eq} values will be used as a reference point for comparing the results obtained using the $Q_{eq\text{-}Semi\text{-}Analytical}$ and $Q_{eq\text{-}Numerical}$.

4.1 Repository model description

The repository model considered in this study consists of 50 deposition holes, a deposition tunnel, and an excavation damaged zone (EDZ). The model employs a representation of the deposition holes as cylinder structures, while the EDZ is conceptualized as a continuous fracture situated beneath the floor of the deposition tunnel, similar to previous studies (Joyce et al. 2010). Figure 4-1 depicts the repository's structural layout, highlighting key elements including deposition holes 24–30, measurement boxes (grey), the deposition tunnel (green), and the EDZ (blue). The graphical representation serves as a visual aid for facilitating the understanding of the repository layout and the spatial relationships between its constituent components.

Table 4-1 provides the properties of the tunnel and EDZ used in the model, including hydraulic conductivity and porosity values that correspond to the buffer properties in each structure. The repository domain is modelled using a network of fractures with appropriate hydraulic and transport properties, which is initially generated in FRACGEN based on the fracture model developed for the site descriptive model of Forsmark (Follin et al. 2007). The fracture network, "seed-12353-500-box-con.fab", is then imported into DarcyTools to represent a connected system of fractures.

Table 4-1 Properties of the Tunnel and EDZ in the Model.

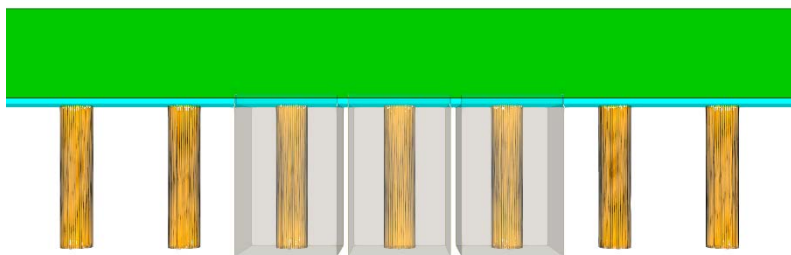| Structure	Height [m]	Width [m]	Hydraulic Conductivity [m/s]
Deposition Tunnel	6.0	4.0	1.0E−10
EDZ	0.3	4.0	3.33E−8

Figure 4-1. *Illustration of the Tunnel (green), EDZ (blue) and measurement boxes (grey) used for capturing the rate of solute transported from deposition hole (orange).*

In DarcyTools, the bedrock is represented as a $500 \times 500 \times 500$ m^3 domain that is initially discretized into a uniform grid with cell sizes of $\Delta x = \Delta y = \Delta z = 2$ m. To improve the accuracy of the numerical solution, a refined mesh is employed in the proximity of the deposition holes, resulting in deposition hole wall cells with a size of 0.125 m, corresponding to a Δ_{wall}/R ratio of 0.14, See Figure 4-2. In the 2D model, as depicted in Figure 2-3, this ratio leads to an approximate −22 % relative error in the numerical results, Q_n, compared to the analytical Q_{eq}. However, in the 3D model, this ratio results in reasonably close $Q_{eq\text{-}Numerical}$ and $Q_{eq\text{-}Semi\text{-}Analytical}$ results, with an approximate −2 % relative error, as demonstrated in Figure 3-2 for Pe = 50. Despite the potential error it may introduce (−22 % as discussed above), this ratio is considered reasonable for application in the large-scale model to achieve reasonably accurate results while avoiding high computational costs.

Since the computational domain is discretized into cell volumes, the fracture network properties are geometrically upscaled onto the grid using the area-weighting method to create a porous medium with equivalent properties. This results in cells with high permeability (mobile cells) and low permeability (immobile cells). The immobile cells are removed from the domain to enhance computational efficiency, as they are not expected to provide flow paths for water to carry solute particles. The upscaling method in DarcyTools is documented in (Ferry, 2020b).

4.2 Boundary conditions

To induce a head gradient of approximately 10^{-3} [m/m], fixed pressure boundary conditions are applied at the inlet (x = −250 m) and outlet (x = 250 m) boundaries. The remaining boundaries of the domain are subjected to a no-flux boundary condition. Based on the above conditions, the total flow rate through the domain is calculated to be 1.27×10^{-7} [m^3/s].

To calculate $Q_{eq\text{-}Numerical}$ around each deposition hole i, the transport model is set up with a unity boundary condition, C = 1, inside the deposition hole i, while a no-flux boundary condition is assigned at the remaining boundaries. It should be noted that this approach results in 50 independent simulation cases, one for each deposition hole.
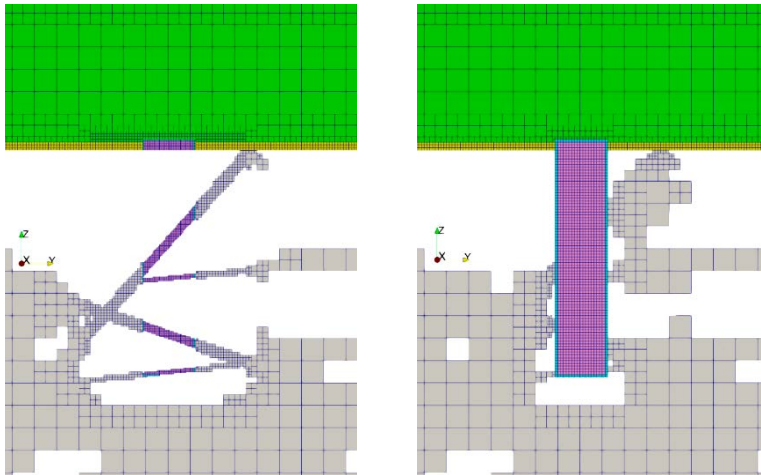

Figure 4-2. *Partial view of y-plane cut at a deposition hole after cell removal for the numerical framework (left), and semi-analytical framework (right).*

4.3   Calculating *Qeq*

Same numerical and semi-analytical frameworks outlined in Sections 3.2.1 and 3.2.2 are employed to calculate $Q_{eq\text{-}Semi\text{-}Analytical}$ and $Q_{eq\text{-}Numerical}$ values. Additionally, corresponding Q_{eq} values obtained from a DFN model implemented in ConnectFlow are presented. These Q_{eq} values are then compared to those obtained using DarcyTools. The results of this comparative analysis are presented in Figure 4-5 to Figure 4-8, encompassing both Q_{eq1}[16] and Q_{eq2}[17].

The findings reveal that approximately 30 % of the deposition holes intersected with conductive fractures, while the remaining holes remain intact. However, it is important to note that solutes can still be released into the EDZ at the top of a deposition hole, contributing to Q_{eq2}. In the studied repository model, Q_{eq1} and Q_{eq2} accounted for 66 % and 34 % of the total release, respectively.

In case of the Q_{eq1}, the $Q_{eq\text{-}Semi\text{-}Analytical}$ approach predicts higher solute transport rates compared to both the $Q_{eq\text{-}Numerical}$ and Q_{eq} obtained using ConnectFlow. Several factors contribute to these differences in results:

1) **$Q_{eq\text{-}Semi\text{-}Analytical}$ Overestimation**: Part of this discrepancy can be attributed to the inherent behaviour of the $Q_{eq\text{-}Semi\text{-}Analytical}$ approach, which tends to overestimate Q_{eq} when a fracture intersects the deposition hole at an angle, refer to Figure 4-3. This phenomenon was demonstrated in Chapter 3 of the report. Additionally, deposition holes 13 and 33, which are only partially intersected by fractures, as shown in Figure 4-3 (bottom), exhibit an overestimation. This overestimation can be attributed to the underlying assumption of the Q_{eq} model, where a fracture fully intersects the deposition hole.

2) **Grid Size Influence:** Another contributing factor is that the $Q_{eq\text{-}Numerical}$ results may have been underestimated due to the use of a relatively large grid size in the simulation. This conclusion is derived from the results of the studies we conducted to explore the sensitivity of $Q_{eq\text{-}Numerical}$ results to variations in grid size, both in 2D and 3D models. Refer to Figure 2-3 and Figure 3-2 for visual representations of the sensitivity analysis results.

3) **Uncertainties in ConnectFlow:** Furthermore, there may be uncertainties associated with the ConnectFlow results that are not fully known to the authors, which can also contribute to the differences observed.

Exception: Deposition Hole 16: Interestingly, when examining deposition hole number 16, the $Q_{eq\text{-}Numerical}$ approach predicts no transport from that hole with $Q_{eq1} = 0$. This is because, as shown in Figure 4-3 (top), a fracture has only intersected the "wall" of the deposition hole 16, resulting in only the properties of the wall boundary cell being updated. Consequently, the properties of the cell located inside the deposition hole remained intact and nonconductive. Thus, during the refinement process, which dictates that only cells intersected by a conductive fracture will remain in the domain, these nonconductive cells were removed from the domain. As a result, the positions of the concentration boundary condition, i.e., cells located inside the deposition hole, do not exist, and the transport equation is not solved, leading to the numerical approach returning zero for $Q_{eq\text{-}Numerical}$. In this case, the $Q_{eq\text{-}Semi\text{-}Analytical}$ approach provides a more accurate estimation of Q_{eq1}. This is because the $Q_{eq\text{-}Semi\text{-}Analytical}$ approach utilizes the flow information from both the inside and wall boundary cells, unlike the $Q_{eq\text{-}Numerical}$, and returns a Q_{eq1} value that is very close to the value obtained using ConnectFlow.

It can also be seen that Q_{eq1} is zero for the deposition holes 34 and onwards. This is primarily because no fracture intersects these deposition holes, leading to $Q_{eq1} = 0$.

In the case of Q_{eq2}, it is important to note that the estimated values obtained using the $Q_{eq\text{-}Semi\text{-}Analytical}$ consistently exceed those obtained using the $Q_{eq\text{-}Numerical}$.

However, in this specific case where the EDZ intersects the deposition hole at a right angle, it has been demonstrated that $Q_{eq\text{-}Semi\text{-}Analytical}$ and $Q_{eq\text{-}Numerical}$ yield comparable results for the given Péclet values, refer to Section 3.2.4. The lower $Q_{eq\text{-}Numerical}$ values in this example can be attributed to the use of a larger wall grid size in the simulation. This increased grid size might result is an underestimation of the $Q_{eq\text{-}Numerical}$ by inadequately representing the boundary conditions with C = 1 on the inside cells.

---

[16] Q_{eq1}: equivalent flow rate to the fracture intersecting the deposition hole.

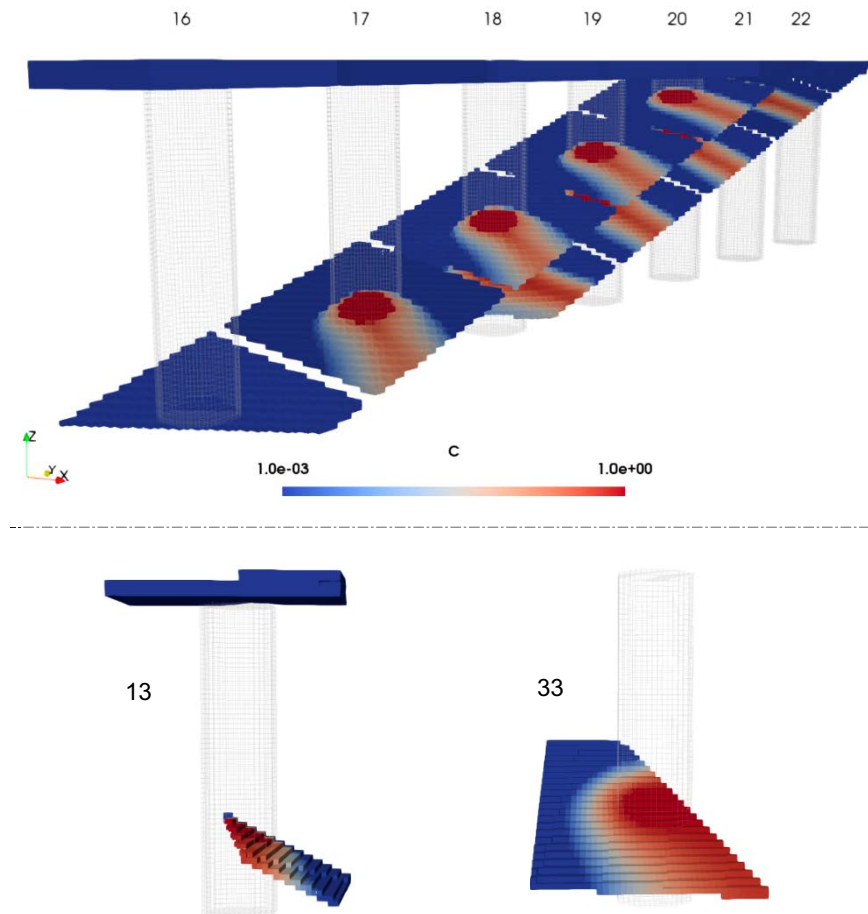[17] Q_{eq2}: equivalent flow rate to the excavation damaged zone.

Figure 4-3. *Solute concentration in the Q_{eq1} measurement boxes used for the solute transport integration of the deposition hole 16–22 (top), 13 (bottom left) and 33 (bottom right) intersected by one or two fractures at angles.*
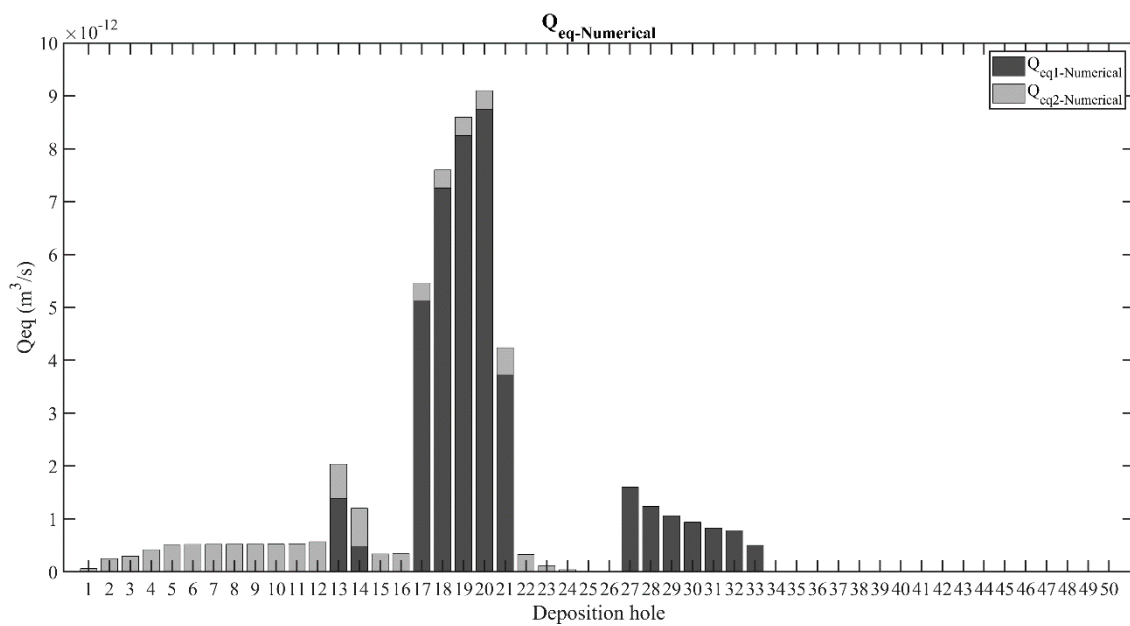

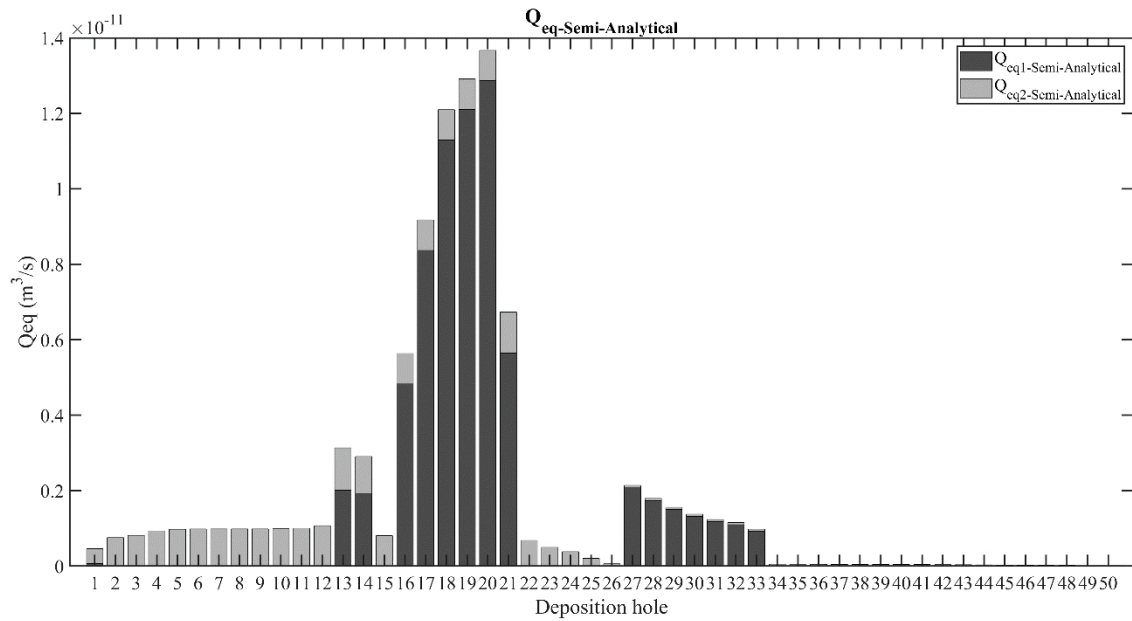**Figure 4-4.** *The solute transport integration results, $Q_{eq\text{-}Numerical}$.*

Figure 4-5. The Semi-Analytical results, $Q_{eq\text{-}Semi\text{-}Analytical}$.

Figure 4-6. Comparison of the Q_{eq1} results obtained from, $Q_{eq\text{-}Numerical}$, $Q_{eq\text{-}Semi\text{-}Analytical}$, and ConnectFlow

For deposition holes 2–18, where the EDZ flow remains unaffected by intersecting fractures, the $Q_{eq\text{-}Semi\text{-}Analytical}$ approach generally returns higher values compared to Q_{eq2} values obtained using ConnectFlow. However, for deposition holes 19–20–22–23 and 24, where a couple of fractures intersect the EDZ, as depicted in Figure 4-7 (top), ConnectFlow predicts notably larger values compared to the $Q_{eq\text{-}Semi\text{-}Analytical}$ approach. The discrepancies in the results could be attributed to differences in how ConnectFlow and DarcyTools handle the situation where multiple fractures intersect the EDZ and how they estimate Q_{eq2}.

Moreover, for deposition holes 25–50, ConnectFlow predicts significantly higher Q_{eq2} values, whereas DarcyTools estimates minimal flow rates in the EDZ sections above these holes, as illustrated in Figure 4-7 (bottom). Consequently, the $Q_{eq-Numerical}$ and $Q_{eq-Semi-Analytical}$ values estimated by DarcyTools become negligible for these deposition holes. However, it is important to note that in this scenario, the estimated Péclet number by DarcyTools falls below the Q_{eq} model's validity range, leading to inaccurate $Q_{eq-Semi-Analytical}$ values, as shown in Figure 4-8.

The variations in the results may also arise from the underlying assumptions, approximations, and methods employed in each approach, as well as how ConnectFlow and DarcyTools model the underlying fracture network. Further investigation is required to fully understand and address these discrepancies between the two modelling approaches and to enhance the accuracy of Q_{eq2} predictions in diverse subsurface conditions, especially in complex intersection scenarios.

Figure 4-7. Solute concentration in the Q_{eq2} measurement boxes used for the solute transport integration of the deposition hole 19–20 (Top) and 30–33 (bottom) intersected by EDZ and a fracture at an angle (20-21-22).
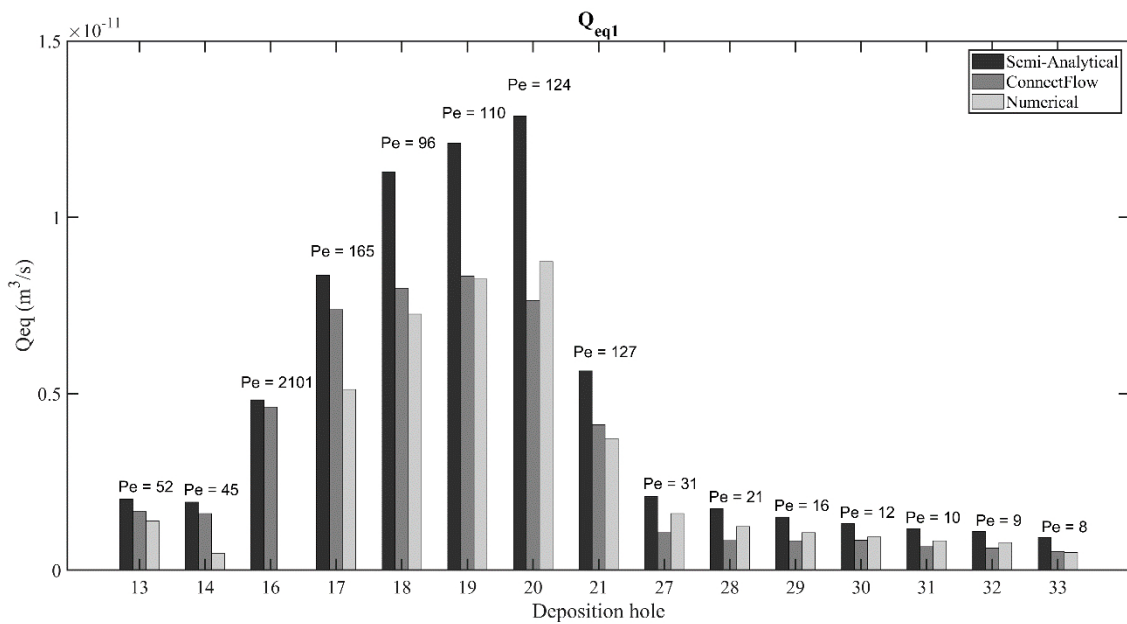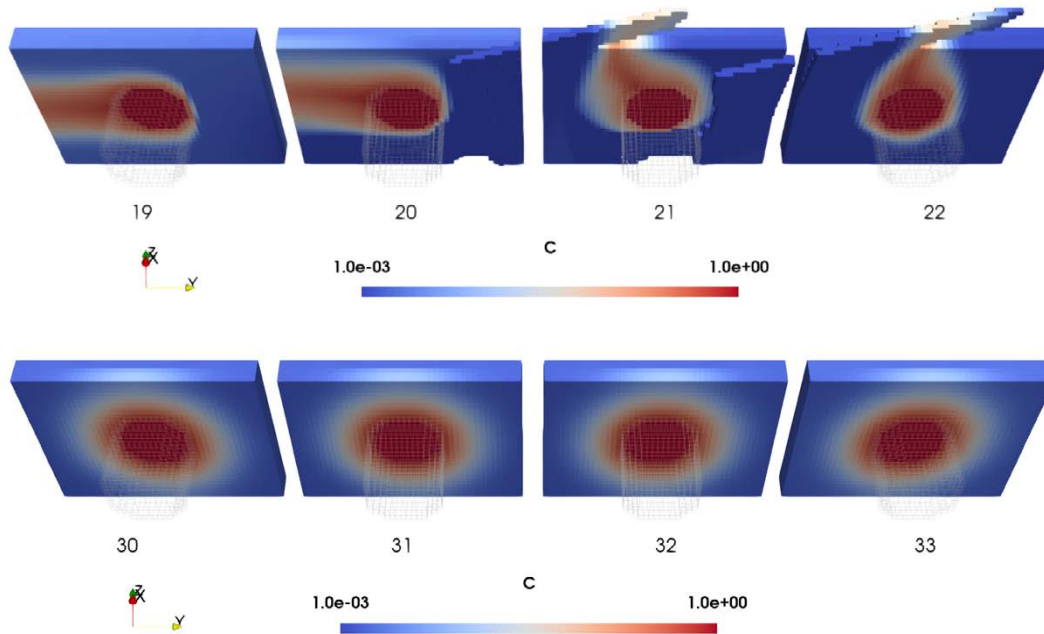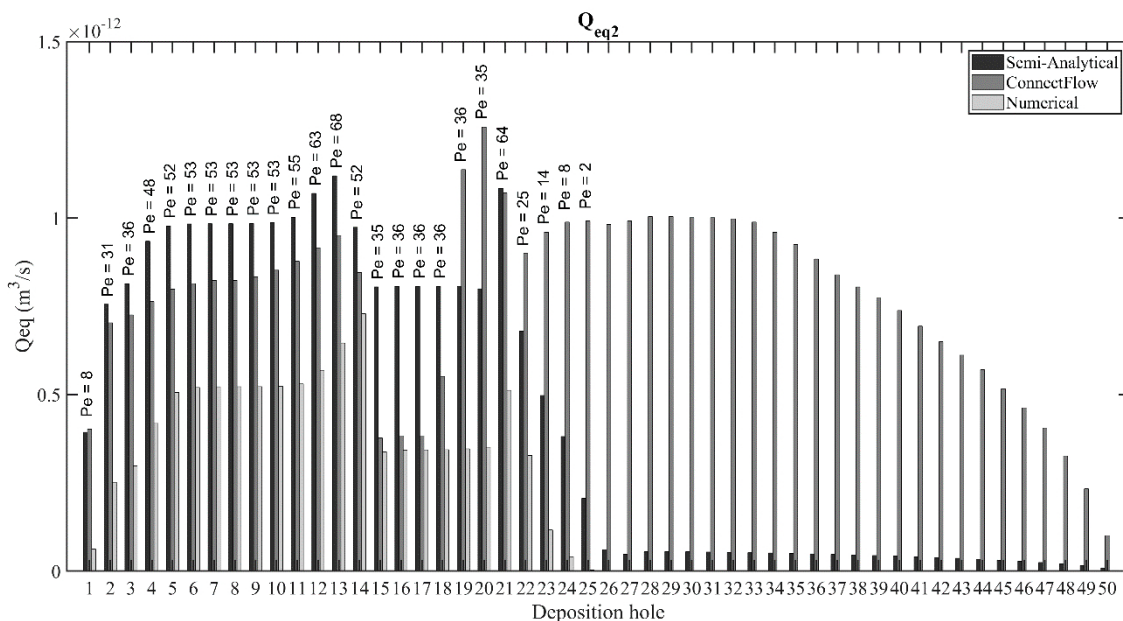

Figure 4-8. Comparison of the Q_{eq2} results obtained from, $Q_{eq-Numerical}$, $Q_{eq-Semi-Analytical}$, and ConnectFlow.

References

SKB's (Svensk Kärnbränslehantering AB) publications can be found at www.skb.com/publications.

Bird R B, Stewart W E, Lightfoot E N, 2002. Transport phenomena, 2nd ed.

Chambré P L, Pigford T H, Fujita A, Kanki T, Kobayashi A, Lung H, Ting D, Sato Y, Zavoshy S J, 1982. Analytical performance models for geologic repositories. LBL-UCB-NE-4017, UC70.

Ferry M, 2020a. FRACGEN, Technical Report TR 19063, MFRDC.

Ferry M, 2020b. GEHYCO, Technical Report TR 20107, MFRDC.

Ferry M, 2020c. Q_{eq} Assessment, Technical Report TR 21051, MFRDC.

Follin S, Levén J, Hartley L, Jackson P, Joyce S, Roberts D, Swift B, 2007. Hydrogeological characterisation and modelling of deformation zones and fracture domains, Forsmark modelling stage 2.2. SKB R-07-48, Svensk Kärnbränslehantering AB.

Joyce S, Simpson T, Hartley L, Applegate D, Hoek J, Jackson P, Swan D, Marsic N, Follin S, 2010. Groundwater flow modelling of periods with temperate climate conditions – Forsmark, Tech. Rep. SKB R-09-20, Svensk Kärnbränslehantering AB.

Neretnieks I, Liu L, Moreno L, 2010. Mass transfer between waste canister and water seeping in rock fractures. Revisiting the Q-equivalent model. SKB TR-10-42, Svensk Kärnbränslehantering AB.

Romero L, 1995. The near-field transport in a repository for high-level nuclear waste, Ph.D. Thesis, TRITA-KET R21, The Royal Institute of Technology, Stockholm, Sweden.

van Brakel J, Heertjes P M, 1974. Analysis of diffusion in macroporous media in terms of a porosity, a tortuosity and a constrictivity factor, International Journal of Heat and Mass Transfer 17 (9). https://doi.org/10.1016/0017-9310(74)90190-2.

A note on the effective diffusivity, D_e

The Fick's law describes the movement of a substance through a medium from a region of higher concentration to a region of lower concentration. It can be written as:

$$J = -D_e \nabla C \tag{A-1}$$

where J is the mass of solute transferred per unit area accessible for diffusion and unit time, D_e is the effective diffusivity and C is the solute concentration. In the case of a porous medium, the effective diffusivity is a measure of the transport properties of the entire medium, while the pore diffusivity (D_p) characterizes the diffusion in the individual pores of the medium. In other words, the effective diffusivity considers the fact that the porous medium has a smaller cross-sectional area available for diffusion than a solid or a fluid without any pores. This means that when a substance diffuses through a porous medium, it encounters obstacles and barriers, such as the solid matrix or the walls of the pores, that reduce the effective cross-sectional area available for diffusion. As a result, the rate of diffusion of the substance through the medium is slower than it would be in the absence of these obstacles, characterized by D_w. The effective diffusivity quantifies this reduction in the rate of diffusion and considers the geometrical characteristics of the porous medium, including its porosity, tortuosity, and constrictivity.

Porosity, ε, is the fraction of the volume that is made up of pores. Tortuosity, τ, is a measure of how tortuous the pore space is, i.e., how much longer the actual path of diffusion is compared to a straight line between two points. Constrictivity, δ, is a measure of how much the pores are constricted, which can limit the movement of solutes through the medium. The relationship between D_e, D_p, D_w, ε, τ, and δ can be expressed as:

$$D_e = D_p \times \varepsilon = D_w \times G \times \varepsilon = D_w \times F \tag{A-2}$$

The parameters G and F are commonly known as the geometry factor and formation factor, respectively. According to the work of van Brakel and Heertjes (1974), the formation factor can be mathematically expressed as:

$$F = \varepsilon \frac{\delta}{\tau^2} = \varepsilon \times G \tag{A-3}$$

Based on the above consideration, it is worth noting that by substituting the definition of D_e into the Equation (1-20), the Q_{eq} expression for a porous fracture can be expressed as:

$$Q_{eq} = 8\Delta \times \sqrt{\frac{R}{\pi}} \times \sqrt{U_d D_w \varepsilon G} \tag{A-4}$$

It is noteworthy that the definition of a fracture "object" in DarcyTools requires careful assignment of transport parameters, including a diffusion coefficient, D_{e_DT}, which include the porosity, θ, and is defined as:

$$D_{e-DT} = D_w \times \theta \tag{A-5}$$

while the porosity θ and the compaction, γ, are given the following dependencies:

$$\theta = \theta_0 \times \gamma \tag{A-6}$$

θ_0 is a reference porosity field given for a reference pressure field. Based on the information presented above, it can be inferred that DarcyTools incorporates the significance of the geometry factor G into γ. This leads to:

$$Q_{eq} = 8\Delta \times \sqrt{\frac{R}{\pi}} \times \sqrt{U_d D_w \theta_0 \gamma} \tag{A-7}$$

The user should be aware of this formulation when calculating Q_{eq} in a fracture or a damaged zone. Note, however that in all the 2D and 3D simulation cases that are simulated in this report using DarcyTools, it is assumed that the fracture (object) is fully open, with $\theta_0 = \gamma = 1$.

Average Q_{eq} in DFN and ECPM

The mathematical analysis presented in this appendix has employed the Cubic law to compute the equivalent flow rate, Q_{eq}, for both the discrete fracture network (DFN) and the equivalent continuum porous medium (ECPM) models, $Q_{eq\text{-}Semi\text{-}Analytical}$. It has been demonstrated that for single fractures or multiple fractures with the same aperture and length, Q_{eq} values for DFN and ECPM models are equivalent. To deal with multiple parallel fractures with varying apertures, both $Q_{eq\text{-}DFN}$ and $Q_{eq\text{-}Semi\text{-}Analytical}$ are expressed in terms of the mean aperture and the relative deviations. The key takeaway is that when minor deviations in aperture result in similar Q_{eq} values for both DFN and ECPM. Consider a single fracture f that completely crosses the deposition hole at a right angle. The equivalent flow rate, Q_{eq}^f can be computed using Equation (B-1). This equation closely resembles Equation (1-22) where L_f for a circular cylinder is substituted with $4R$[18].

$$Q_{eq}^f = 2b_f \sqrt{\frac{4D_w L_f}{\pi}} \times \sqrt{U_{d,f}} \tag{B-1}$$

In the above equation

- $U_{d,f}$ is the Darcy flux in the fully open fracture f, [m/s].

- b_f is the aperture of the fully open fracture f, [m].

- L_f is the transport distance along the intersection of the circular deposition hole and the fracture f, [m], (see Section 1.4).

- D_w is the diffusivity in water, [m²/s].

If multiple fractures cross the deposition hole, the total $Q_{eq\text{-}DFN}$ is the sum of the fluxes through the nf fractures:

$$Q_{eq-DFN} = \sum_{f=1}^{nf} Q_{eq}^f = 2 \times \sum_{i=1}^{nf} b_f \sqrt{U_{d,f}} \sqrt{\frac{4D_w L_f}{\pi}} \tag{B-2}$$

For parallel fractures, the transport length is constant and denoted as L.

$$L_f = L \tag{B-3}$$

Assuming flow in the fractures follows the "Cubic law" and uniform pressure gradient across all fractures, we can express Darcy flux using Equation (B-4):

$$U_{d,f} = \frac{Q_f}{A_f} = k_f \beta = \frac{b_f^2}{12} \beta \tag{B-4}$$

where:

- k_f represent the permeability of fracture f, [m²].

- β denotes the pressure gradient divided by the dynamic viscosity, [m^{-1}s^{-1}].

Using the above two assumptions, we can reformulate Equation (B-2) to give:

$$Q_{eq-DFN} = \sum_{f=1}^{nf} Q_{eq}^f = 2 \times \sqrt{\frac{\beta D_w L_f}{3\pi} \sum_{i=1}^{nf} b_f^2} \tag{B-5}$$

---

[18] This is to address velocity differences among adjacent streamlines close to the deposition hole, as elaborated in Section 1.5.

Now let's consider the ECPM approximation of Q_{eq}, as expressed by the semi-analytical solution Equation (1-34), (Note that in Equation (1-34) $L_f = 4R$):

$$Q_{eq-Semi-Analytical} = 2H \sqrt{\frac{4D_w L}{\pi}} \sqrt{\theta_M U_M} \tag{B-6}$$

θ_M for the case of parallel fractures can be computed as:

$$\theta_M = \frac{1}{H} \sum_{i=1}^{nf} b_f \tag{B-7}$$

U_M can be obtained using the following expression:

$$U_M = \sum_{i=1}^{nf} \frac{k_f b_f}{H} = \frac{\beta}{12H} \sum_{i=1}^{nf} b_f^3 = k_M \beta \tag{B-8}$$

Where k_M represents the mean permeability. Substituting θ_M and U_M in the $Q_{eq-Semi-Analytical}$ expression results in:

$$Q_{eq-Semi-Analytical} = 2 \sqrt{\frac{\beta D_w L}{3\pi}} \sqrt{\sum_{i=1}^{nf} b_f \sum_{i=1}^{nf} b_f^3} \tag{B-9}$$

In case of a single fracture ($nf = 1$) or several fractures with the same aperture ($b_f = b$) and length ($L_f = L$), the Q_{eq} values for DFN and ECPM are identical and can be expressed as:

$$Q_{eq-Semi-Analytical} = Q_{eq-DFN} = 2 \times nf \times \sqrt{\frac{\beta D_w L}{3\pi}} b^2 \tag{B-10}$$

In case of several fractures sharing the same length ($L_f = L$), but having different apertures, Q_{eq-DFN} and $Q_{eq-Semi-Analytical}$ can be expressed as a function of the mean aperture, b_M and the relative deviations, σ, as defined below:

$$b_M = \frac{1}{nf} \sum_{i=1}^{nf} b_f \tag{B-11}$$

and

$$\sigma_f = \frac{b_f - b_M}{b_M} \tag{B-12}$$

Consequently, Q_{eq-DFN} and $Q_{eq-Semi-Analytical}$ can be expressed as a

$$Q_{eq-DFN} = \sum_{f=1}^{nf} Q_{eq}^f = 2 \times nf \times b_M^2 \sqrt{\frac{\beta D_w L_f}{3\pi}} \left(1 + \frac{1}{nf} \sum_{i=1}^{nf} \sigma_f^2 \right) \tag{B-13}$$

$$Q_{eq-Semi-Analytical} = 2 \times nf \times b_M^2 \sqrt{\frac{\beta D_w L_f}{3\pi}} \sqrt{\left(1 + \frac{3}{nf} \sum_{i=1}^{nf} \sigma_f^2 + \frac{1}{nf} \sum_{i=1}^{nf} \sigma_f^3 \right)} \tag{B-14}$$

From the two equations above, it can be inferred that when small deviations ($\sigma_f \ll 1$) are present, both DFN and ECPM yields similar Q_{eq} values.

Equivalent Darcy Flux in DFN and ECPM

In DFN models, where properties of individual fractures are available, a 2D Darcy flux has been defined as the flow per unit width of the fracture:

$$U_{2D} = \frac{Q_f}{\sqrt{a_f}} \tag{C-1}$$

Q_f represents the flow rate in fracture f, and a_f denotes the area of the fracture. Thus $\sqrt{a_f}$ can be seen as a measure of the length of a side. The flow velocity in the fracture can then be obtain from:

$$u = \frac{Q_f}{b_f \sqrt{a_f}} \tag{C-2}$$

b_f is the aperture of fracture f. The Q_{eq} formulation for the discrete fracture network representation of the parallel fractures intersecting the deposition hole is given by Equation (1-24):

$$Q_{eq-DFN} = \frac{8\sqrt{D_w R}}{\sqrt{\pi}} \times H \times \left[\frac{1}{H} \times \sum_{i=1}^{nf} b_f \sqrt{u} \right] \tag{C-3}$$

Equation (C-3) is similar to equation D-8 in (Joyce et al. 2010). If use definition of u as given in Equation (C-2), Q_{eq_DFN} becomes:

$$Q_{eq-DFN} = \frac{8\sqrt{D_w R}}{\sqrt{\pi}} \times H \times \left[\frac{1}{H} \times \sum_{i=1}^{nf} \sqrt{b_f \frac{Q_f}{\sqrt{a_f}}} \right] \tag{C-4}$$

Here, H represents the height of the deposition hole. We can also define the following term as the equivalent $\sqrt{u}$ in the vicinity of the deposition hole:

$$\left(\sqrt{u} \right)_{eq} = \frac{1}{H} \times \sum_{i=1}^{nf} b_f \sqrt{u} \tag{C-5}$$

The primary objective here is to derive an estimate for U_{2D} by using the ECPM formulation presented in this study, Equation (C-6):

$$Q_{eq,ECPM} = \frac{8\sqrt{D_w R}}{\sqrt{\pi}} \times H \times \left(\sqrt{\theta U} \right)_{M-ECPM} \tag{C-6}$$

By comparing Equation (C-4) with Equation (C-6), and considering the approximation of $Q_{eq,ECPM}$ with $Q_{eq\text{-}Semi\text{-}Analytical}$, given in Equation (1-34), it can be understood that:

$$\left(\sqrt{u} \right)_{eq} = \left(\sqrt{\theta U} \right)_{M-ECPM} \approx \sqrt{\theta_M U_M} \tag{C-7}$$

However, it is important to note that Equation (C-7) solely provides information regarding equivalent $\sqrt{u}$. Nonetheless, we aim to estimate the equivalent Darcy flux u. This raises the question: How can we effectively deduce u_{eq} from $\left(\sqrt{u} \right)_{eq}$?

We illustrate this process for two known distributions for $\sqrt{u}$, namely, normal, and lognormal distribution. Let's consider the following transformation of variables:

$$x = \sqrt{u} \tag{C-8}$$

Consequently,

$$x^2 = u \tag{C-9}$$

This leads to expressing the mean (expected) values as follows:

$$(\sqrt{u})_{eq} = E[x]$$ (C-10)

and

$$u_{eq} = E[x^2]$$ (C-11)

If x follows a **normal distribution** with a mean μ and a standard deviation σ, then the mean of x, $E[x]$, and the mean of x^2, $E[x^2]$, can be, respectively, expressed as:

$$E[x] = \mu$$ (C-12)

$$E[x^2] = \mu^2 + \sigma^2 = (E[x])^2 + \sigma^2$$ (C-13)

Alternatively, if we assume that x follows a **log-normal distribution** with a mean of μ and a standard deviation of σ, then the mean of x, $E[x]$, can be calculated as:

$$E[x] = \exp\left(\mu + \frac{\sigma^2}{2}\right)$$ (C-14)

Similarly, the mean of x^2, $E[x^2]$, can be expressed as:

$$E[x^2] = \exp\left(2\mu + 2\sigma^2\right) = (E[x])^2 \times \exp\left(\sigma^2\right)$$ (C-15)

It may be noted that in both cases if the variance of x, σ^2, is small then.

$$E[x^2] \approx (E[x])^2$$ (C-16)

Hence, considering Equation (C-7), we can express $E[x^2]$ as follows:

$$E[x^2] = u_{eq} \approx \left((\sqrt{u})_{eq}\right)^2 \approx \theta_M \times U_M$$ (C-17)

In the above equations, σ^2 represents the variance of $\sqrt{u}$. Consequently, *it is only when σ^2 is small*, indicating that the fracture velocities are comparable, we can deduce:

$$(\sqrt{u})_{eq} = \frac{1}{H} \times \sum_{i=1}^{nf} b_f \sqrt{u} = \frac{1}{H} \times \sum_{i=1}^{nf} \sqrt{b_f \frac{Q_f}{\sqrt{a_f}}} \approx \sqrt{\theta_M \times U_M}$$ (C-18)

The quantity $\sum_{i=1}^{nf} \sqrt{b_f \frac{Q_f}{\sqrt{a_f}}}$ can then be computed as:

$$\sum_{i=1}^{nf} \sqrt{b_f \frac{Q_f}{\sqrt{a_f}}} \approx \sqrt{\theta_M \times U_M \times H^2}$$ (C-19)

For a single fracture that intersect the deposition hole at a right angle:

$$\frac{Q_f}{\sqrt{a_f}} \approx \theta_M \times U_M \times \frac{H^2}{b_f}$$ (C-20)

Using Equation (1-40) and (1-41) for θ_M and U_M for a single fracture intersecting the deposition hole at a right angle leads to,

$$U_{2D} = \frac{Q_f}{\sqrt{a_f}} \approx \frac{b_f}{H} \times \frac{b_f}{H} u \times \frac{H^2}{b_f} = b_f u$$ (C-21)

Tests with alternative geometries

The Q_{eq} analytical solution for a circular deposition hole is given by Equation (1-21). To apply this solution to other deposition hole geometries, not just circular ones, it is necessary to use an equivalent radius for the inclusion instead of the radius (R) in Equation (1-21). This equivalent radius, denoted as R_e, represents the radius of a hypothetical circular cylinder that has the same area as the inclusion. R_e can be defined using the formula:

$$R_e = \frac{S}{\sqrt{\pi}} \tag{D-1}$$

where S [m^2] denotes the area of the intersection between the inclusion and the deposition surface.

Hence, an analogous Péclet analysis, as the one carried out in Section 2.3 for a circular deposition hole, can also be conducted for square and elliptical-shaped deposition holes.

The results of this new study show that there is a similar range of Péclet values ($4 < Pe < 700$) where Q_n obtained through numerical integration and Q_{eq} agree for both square and elliptical-shaped deposition holes.
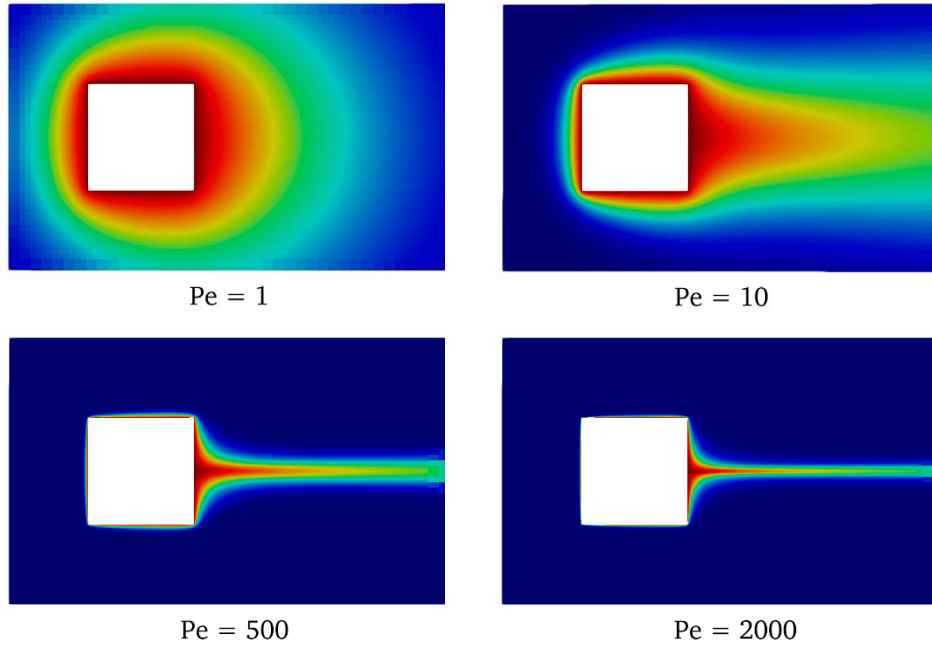

Pe = 1

Pe = 10

Pe = 500

Pe = 2000

Figure D-1. *Solute concentration profile around a deposition hole with a square cross-section area at different Péclet numbers.*

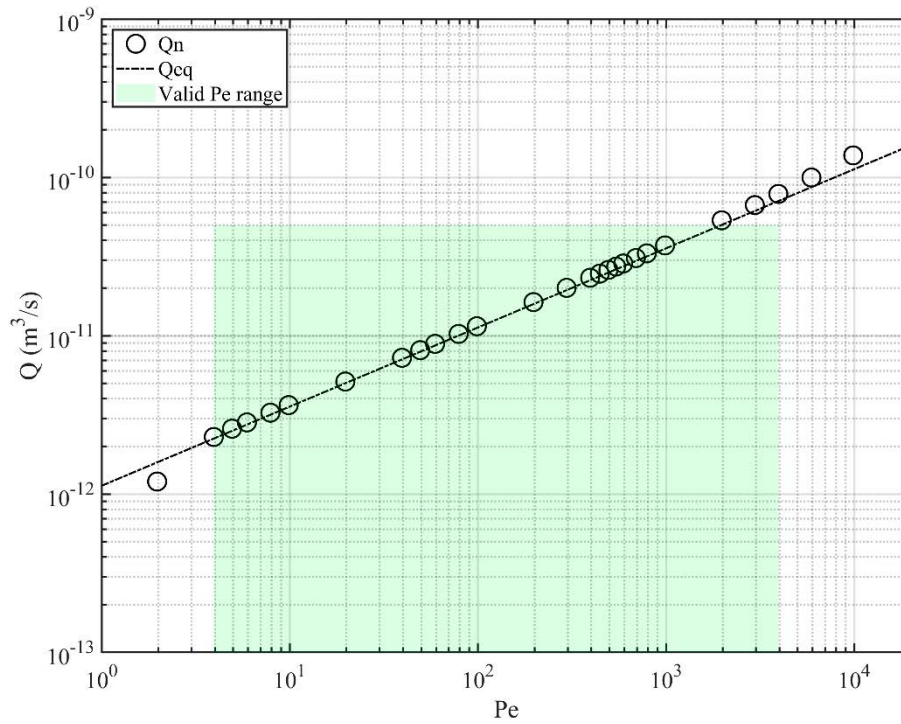**Figure D-2.** *Estimated Q_{eq} values at different Péclet number for a deposition hole with square cross-section area. $\Delta_{wall}/R = 7 \times 10^{-4}$. The green zone indicates where the relative error between Q_n and Q_{eq} is less than 10 %.*

Figure D-3. *Solute concentration profile around a deposition hole with an elliptical cross-section area at different Péclet numbers.*

Figure D-4. *Estimated Q_{eq} values at different Péclet number for a deposition hole with elliptical cross-section area. $\Delta_{wall}/R = 7 \times 10^{-4}$. The green zone indicates where the relative error between Q_n and Q_{eq} is less than 10 %.*
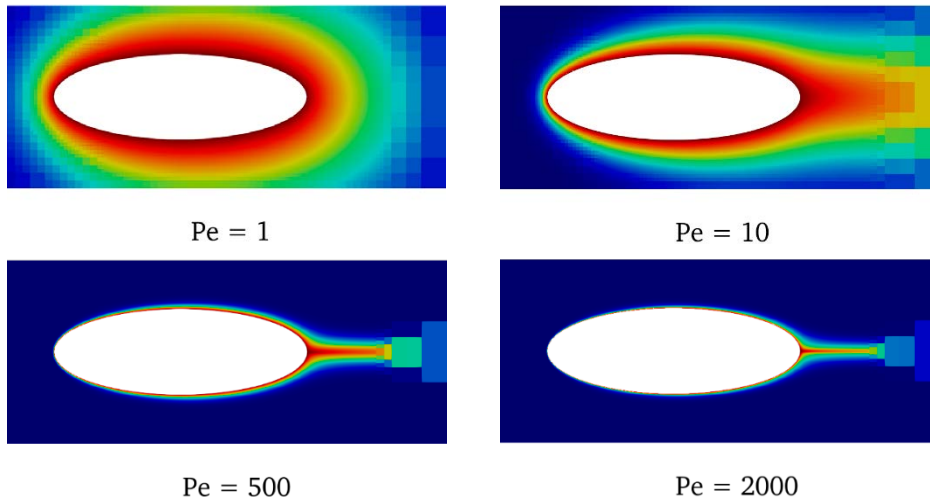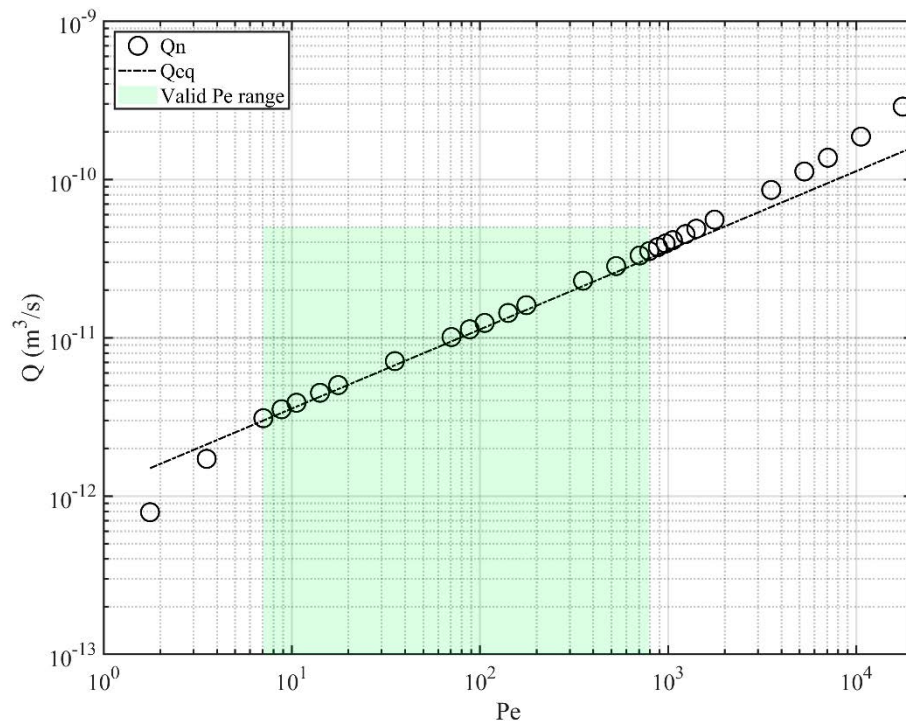
Nomenclature

Symbol	Description	Unit
A_k	Surface area of a DT cell normal to k-direction	m²
C	Concentration	mol/m³
C_0	Concentration at water-buffer interface	mol/m³
D_e	Effective diffusivity	m²/s
D_p	Pore diffusivity	m²/s
D_w	Diffusivity in water	m²/s
F	Formation factor	-
G	Geometry factor	-
H	Height of the deposition hole	m
J	Diffusion flux	mol/m²s
L	Distance travelled by fluid	m
Q	Volumetric flow rate	m³/s
Q_{eq}	Equivalent flow rate	m³/s
$Q_{eq\text{-}DFN}$	Average equivalent flow rate from DFN conceptualisation	m³/s
$Q_{eq\text{-}Numerical}$	Equivalent flow rate from numerical implementations	m³/s
$Q_{eq\text{-}Semi\text{-}Analytical}$	Equivalent flow rate from semi-analytical method	m³/s
$Q_{eq\text{-}2D\text{-}Analytical}$	Equivalent flow rate in the 2D model from analytical method	m³/s
R	Radius of the cylinder/deposition hole	m
T	Dimensionless group characterizing the spreading rate of solute	-
U_d	Darcy flux	m/s
$U_{d,f}$	Darcy flux in fully open fracture f	m/s
U_i	Darcy flux in DT cell i	m/s
U_M	Mean Darcy flux of selected cells in DT domain	m/s
U_{2D}	Flow rate per unit width of the fracture	m²/s
V_f	Volume of fluid	m³
α_f	Area of fracture f	m²
b_f	Aperture of fully open fracture f	m
c_m	Mean Concentration of water	mol/m³
c_w	Concentration of water	mol/m³
h	Hydraulic head gradient	m/m
nc	Number of DT cells within a fracture intersection	-
$\vec{n}$	Normal vector	-
t_{mix}	Time for domain to reach a well-mixed condition	s
t_{res}	Water residence time in contact with the surface	s
u	True fluid velocity	m/s
u_k	Darcy flux on DT cells' surfaces. Subscript k denotes the flow direction	m/s
$\vec{u}$	Darcy flux vector	m/s
Δ	Thickness of a fracture or a damaged zone	m
Δ_{wall}	Size of a wall boundary cell in the 2D model in DT domain	m
δ	Constrictivity of a porous medium	-
ε	Porosity of fracture (when fracture is assumed porous)	-
ϵ	Estimated error between different Qeq values	m³/s

γ	Compaction of a porous medium, i.e., rock matrix	-
n_{mean}^{FS}	Mean penetration depth	m
θ_i	Porosity of DT cell i	-
θ_M	Mean cell porosity of selected cells in DT domain	-
v_i	Volume of DT cell i	m³
α	Angle of fracture intersection with deposition hole	degree

Abbreviation	Meaning
BC	Boundary condition
DH	Deposition Hole
DFN	Discrete Fracture Network
DT	DarcyTools
ECPM	Equivalent Continuous Porous Medium
EDZ	Excavation Damaged Zone
Pe	Péclet Number
PM	Performance Measures
Qeq	Equivalent flow rate
QA	$Q_{eq\text{-}2D\text{-}Analytical}$
Qn	$Q_{eq\text{-}Numerical}$ in 2D model
QN	$Q_{eq\text{-}Numerical}$ in 3D model
QS	$Q_{eq\text{-}Semi\text{-}Analytical}$ in 3D model

Sample Q_{eq} model codes from CIF-FIF files

```
<cif>

<run>

<title>  'Qeq_Semi_Analytical calculation'  </title>

<griddir> '..\Grid\grids'    </griddir>

</run>

<law_mu><a0> 1.E-3       </a0> </law_mu>

<var> <name> permx     </name> <inifile> '..\Prop\properties/PERMX' </inifile> </var>

<var> <name> permy     </name> <inifile> '..\Prop\properties/PERMY' </inifile> </var>

<var> <name> permz     </name> <inifile> '..\Prop\properties/PERMZ' </inifile> </var>

<var> <name> poros     </name> <inifile> '..\Prop\properties/PORO' </inifile> </var>

<var> <name> stora     </name> <inifile> '..\Prop\properties/STORA' </inifile> </var>


<var> <name> darcy-u   </name> <pos> xface </pos> </var>

<var> <name> darcy-v   </name> <pos> yface </pos> </var>

<var> <name> darcy-w    </name> <pos> zface </pos> </var>

<var> <name> pressure   </name> <pos> cell </pos> </var>


<var> <name>  Uxyz     </name> <ini> domain 0.0 </ini> </var>

<var> <name>  Porm     </name> <ini> domain 0.0 </ini> </var>


<flux> <name> UxE     </name> <loc> Q1-DH </loc> <faces> east  </faces> <type> 'vfl' </type>
</flux>

<flux> <name> UxW      </name> <loc> Q1-DH </loc> <faces> west  </faces> <type> 'vfl' </
type> </flux>

<flux> <name> UyN      </name> <loc> Q1-DH </loc> <faces> north </faces> <type> 'vfl' </type>
</flux>

<flux> <name> UyS     </name> <loc> Q1-DH </loc> <faces> south </faces> <type> 'vfl' </type>
</flux>

<flux> <name> UzL     </name> <loc> Q1-DH </loc> <faces> low   </faces> <type> 'vfl' </type>
</flux>

<flux> <name> UzH     </name> <loc> Q1-DH </loc> <faces> high  </faces> <type> 'vfl' </type>
</flux>


<loc>  <name> Q1-DH   </name> <file>'../Grid/locations/DH.loc' </file></loc>

<loop> <name> main     </name> </loop>
```

```
<slv> <restart> T          </restart> </slv>

</cif>

subroutine usrout(eventname)

use M_UTIL

character(len=*), intent(in) :: eventname

real, dimension(:), pointer :: uxe,uxw,uyn,uys,uzl,uzh

real, dimension(:), pointer :: umxy, porm

real :: Pe, qeq_sa


*..... Is xecuted only at the start of the computation.

if(eventname.ne.'dts_start') return

r = 0.875       !Radius of DH.

dw = 1.E-9       !Water diffusivity.

w = 8.2         !Height of DH.


*..... Retrieve the values of Darcy fluxes in each direction.

uxe  => GET_VAR_VAL('UxE')

uxw  => GET_VAR_VAL('UxW')

uyn  => GET_VAR_VAL('UyN')

uys  => GET_VAR_VAL('UyS')

uzl  => GET_VAR_VAL('UzL')

uzh  => GET_VAR_VAL('UzH')

umxy => GET_VAR_VAL('Uxyz')

porm => GET_VAR_VAL('Porm')


*..... Calculate the mean Darcy flux, denoted as U_M in the report.

umxy    = sqrt((0.5*(uxe-uxw))**2 + (0.5*(uyn-uys))**2 + (0.5*(uzl-uzh))**2)


*..... Calculate the mean porosity, denoted as theta_M in the report.

porm    = GET_VAR_MEAN('poros','Q1-DH')


*..... Calculate the Qeq_Semi_Analytical.

qeq_sa  = 4.51*w*sqrt(dw*r*umxy(1)*porm(1))

end subroutine
```

SKB is responsible for managing spent nuclear fuel and radioactive waste produced by the Swedish nuclear power plants such that man and the environment are protected in the near and distant future.

skb.se